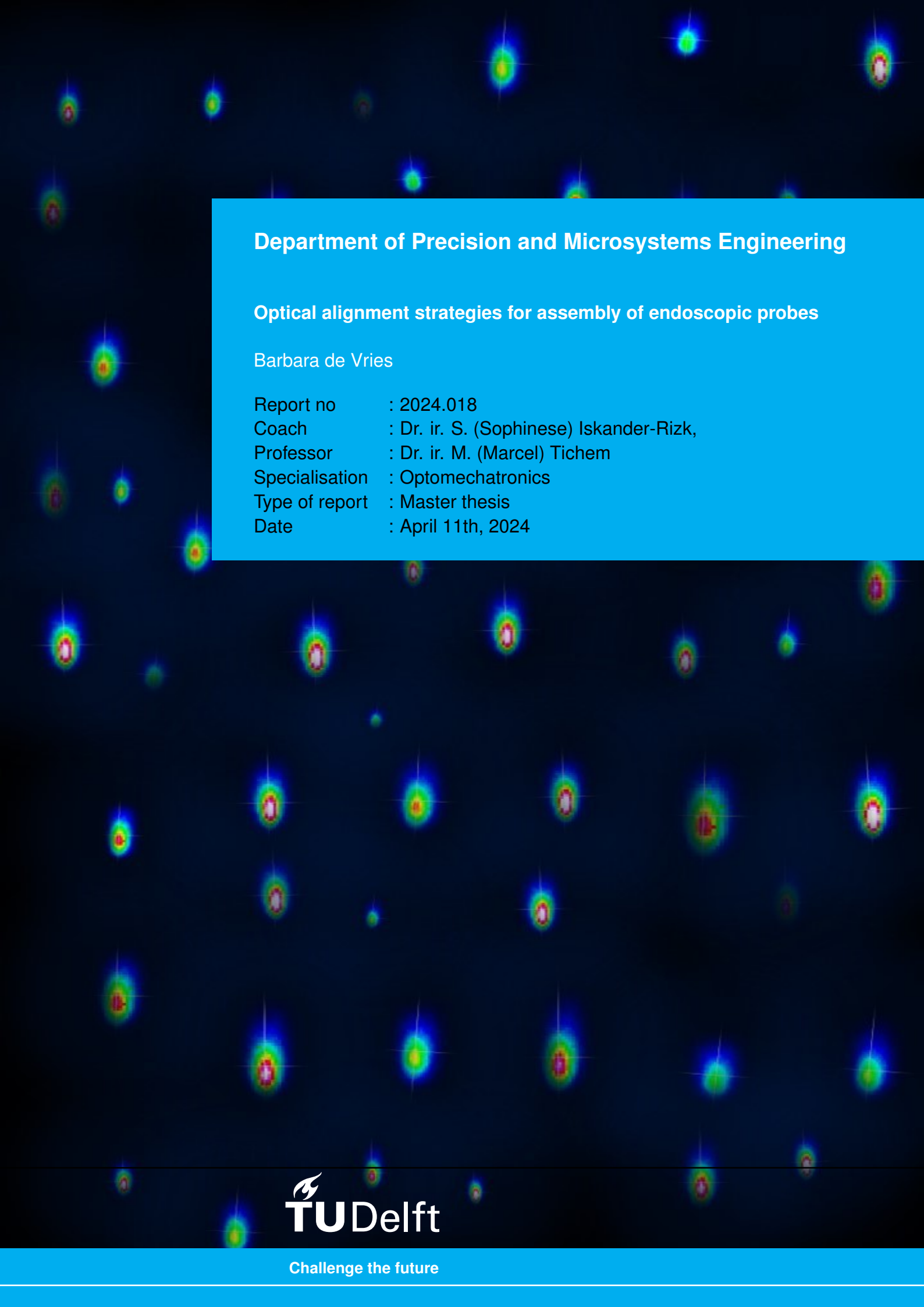

Department of Precision and Microsystems Engineering

Optical alignment strategies for assembly of endoscopic probes

Barbara de Vries

Report no	: 2024.018
Coach	: Dr. ir. S. (Sophinese) Iskander-Rizk,
Professor	: Dr. ir. M. (Marcel) Tichem
Specialisation	: Optomechatronics
Type of report	: Master thesis
Date	: April 11th, 2024

TU Delft

Challenge the future

Optical alignment strategies for assembly of endoscopic probes

by

B.E. de Vries

in partial fulfillment of the requirements for the degree of
Master of Science in Mechanical Engineering at the Delft University of Technology,
to be defended publicly on Thursday April 11th, 2024 at 12:30.

Student number:	4583507	
Project duration:	Feb 6, 2023 – April 11, 2024	
Thesis committee:	Dr. ir. M. (Marcel) Tichem,	TU Delft, supervisor
	Dr. ir. S. (Sophinese) Iskander-Rizk,	TU Delft, supervisor
	Dr. N. (Nandini) Bhattacharya,	TU Delft
	Prof. dr. G. (Gijs) van Soest,	Erasmus MC

TU Delft

Abstract

Reliable assembly methods are needed to translate new endoscopic probes from the research phase to clinical testing. Design variation complicates standardized assembly and leads to a lengthy process creating inaccurate prototypes, preventing repeatable research. This thesis proposes a strategy for selecting the most effective assembly method by examining alignment and bonding relations among parts. Considering the manufacturing tolerances of the optical parts leading to a loss of image quality, an approach for testing is selected to align the gradient index (GRIN) lens and fibre. This approach implements an active alignment procedure and reaches a sensitivity of $3\mu m$ for the concentricity, 0.4^{o} for the colinearity and $40\mu m$ for the separation distance. These results validate a better result than reachable with passive alignment. An optimization algorithm could replace the manual comparison of the ideal beam profile for increased repeatability. To advance the research to the assembly of complete prototypes, more components of the probes should be added to the investigation and a method for fixing the components to the housing should be introduced.

Preface

This thesis translates concepts from mechanical engineering to improve the assembly of medical technology. Although this study does not focus on the medical results, there is great potential to positively impact the future trajectory of medical technology.

The field of surgery is shifting to minimally invasive methods, demanding new and improved imaging devices. The research on these devices, particularly endoscopic probes, has revolutionized not only surgical procedures but also diagnosis and treatment procedures.

This thesis contributes to a specific step in the research process, limiting the advancement of endoscopic probe technologies. Despite remarkable progress in manufacturing techniques, the assembly of endoscopic probe prototypes remains challenging.

My interest arose when research on this topic was hard to find, and every prototype seemed to have its specific assembly method. Through a thorough analysis of the components in the probe prototypes and a standardised approach, the goal was to increase the possible emergence of innovative designs.

In the process of reaching this goal, I had a lot of interesting discussions, with sometimes fascinating conclusions or revelations. For these, I need to thank Marcel Tichem, who gave me the trust and confidence to find my own path in the field of endoscopic probes, sometimes unknown to us both. And when we were unaware, Sophinese Iskander-Rizk was always there, to keep us focused on the medical goals of the endoscopic probes. Although we didn't always see eye-to-eye on what the best improvements were, I hope this thesis will contribute to both your view and anyone else interested in the assembly of endoscopic probes. Thank you for helping me write this thesis, your feedback was greatly appreciated!

Also, I will thank Wieke, for helping me with programming, when I didn't know how to continue, and Christian, for taking the time to proofread some chapters during his already busy days.

Finally, I would like to thank the committee in advance, for taking the time to read this thesis and join the defense. Your effort is very much appreciated.

B.E. de Vries
Delft, January 2013

Contents

1 Introduction

1.1. Technical improvement of endoscopic devices

The field of surgery has changed significantly over the past few decades, with minimally invasive surgery (MIS) standing out as a groundbreaking innovation. MIS involves making a small incision through which the entire surgery is performed, accomplishing a lower impact on patients than traditional surgery. The patient's recovery time is reduced, as is the number of complications [11]. In addition to the improved patient experience, the surgery costs are significantly reduced. During surgery, visual feedback is not direct but is usually generated by an image on a screen.

With the introduction of imaging instruments, new challenges and opportunities arose [8], leading to the emergence of a distinct research domain. Particularly optical biopsy, a method for characterizing tissue during surgery and diagnostics, has revolutionized early disease detection [8], and patients can be diagnosed and treated earlier. When a disease has not yet developed, treatments are less complicated and shorter, and therefore beneficial for patients and healthcare institutions [10]. Consequently, instruments developed for MIS were implemented in additional fields in the clinical area, creating a separate research field and advancing innovation in imaging systems. These imaging instruments primarily consist of distal-end endoscopes, referring to the general term for a viewing system inside the human body, with the imaging system at the distal end that enters the body. The distal end usually consists of a probe, a tubular housing with all the parts inside. The probe is connected to an endoscopic device to create an image that can be used.

While these instruments serve the common function of imaging internal tissues, they vary in size and modality (their working principle) to facilitate imaging for different anatomical structures and diseases. For all instruments, it is generally accepted that smaller sizes allow greater manoeuvrability within the body, facilitating imaging of additional areas [14]. Recent advancements in miniaturization driven by breakthroughs in electronics, computing, and manufacturing techniques such as 3D printing, have significantly enhanced the capabilities of endoscopic probes [1]. However, as endoscopic probes continue to decrease in size, new challenges such as assembly complexities arise, necessitating further research and development [12, 5]. The different imaging modalities show identical functions when abstracted into generalized functionality [16]. These functions include sending the signal, focusing the signal beam, redirecting the signal beam, receiving the signal and rotating the probe [16]. In Figure 1.1, a standard probe design with the most common and essential parts is shown.

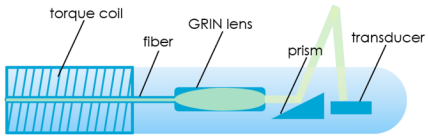

Figure 1.1: Endoscopic probe with functional parts indicated

(a) Example of a side-by-side layout

(b) Example of a sequential layout

Figure 1.2: Example of two different layouts

1.2. Assembly of endoscopic probe prototypes

Even though the components of probes are standard, designs vary substantially. This variation is partly due to the layout and arrangement. The layout determines whether parts are placed for example sequentially or side-by-side [19] as shown in Figure 1.2. Although these designs have a significant difference the arrangement, determined by the alignment relations, remains relatively consistent. Most endoscopes show that the alignment relation between the components is the same. This is very sensible as the signal always follows a certain path, along all parts. A liaison graph showing the most common relation is shown in Figure 1.3 [16]. This knowledge influences the assembly of the endoscopic probe prototypes as the parts do not have an alignment relation with the housing.

The current assembly methods are mostly divisible into three categories. The first and most used method is the use of tubes and glue. The tubes are used for the alignment and are connected to the parts [3]. Extra parts are introduced to do this correctly. It is likely to assume this extra part can cause additional alignment errors and extra handling, complicating the assembly process. Another method is the use of a 3D-printed housing. This method of assembly eases the manufacturing of the housing and is very flexible [2]. Finally, the usage of a silicon optical bench (SiOB) is tested for assembly. Although it shows greater precision, the diameter of the probe becomes very large compared to the parts because of the square dimensions of the SiOB that are encapsulated into a cylinder. This leads to a reduced possibility of miniaturization, which is unwanted [18].

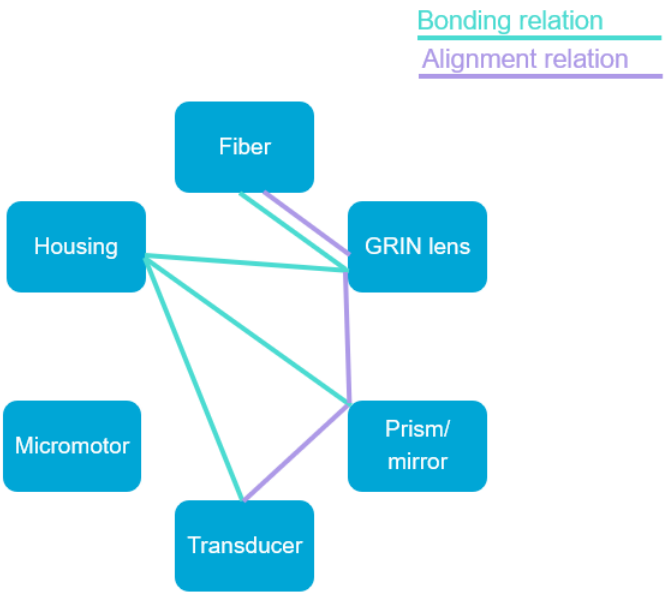

Figure 1.3: Liaison graph applicable to most designs

1.3. Problem statement

Despite significant advancements in endoscopic imaging modalities and manufacturing techniques, the integration of assembly techniques for endoscopic probe prototypes is still in progress.

Thus far, these methods are relatively new, lack a systematic approach, are specific and often only applicable to one innovative design. This specificity results in a delay which could be reduced by a generic assembly technique, simplifying the creation of prototypes and accelerating innovation. Implementing a systematic design approach could bring significant improvements. This leads to the following research goal:

This study aims to develop and assess a strategy to effectively select an assembly process for the optical parts in endoscopic probes. This strategy should address the assembly order and active alignment while prioritizing precision, repeatability, and the challenges associated with miniaturized parts and small series production.

1.4. Thesis structure

This research goal contains the following subgoals which are structured in the report as follows:
The first subgoal is to create and evaluate an overview of possible assembly orders (Chapter 2). A preferred one is selected from these assembly orders, and an assembly method allowing active alignment is designed (Chapter 3). Next, the assembly method is evaluated (Chapter 4) for its precision and repeatability. The results are discussed (Chapter 5) leading to a conclusion and recommendations for further research (Chapter 6).

2

Probe System Examination

This chapter analyses the optical system of an endoscope (the fibre, GRIN lens and prism) to select the preferred assembly order. This leads to selecting active alignment of the fibre and GRIN lens as the assembly step for optimization. The ideal optical path is explained and the influence of alignment errors is investigated to arrive at this conclusion. Then, the manufacturing tolerances of the fibre and GRIN lens are stated and the necessary alignment accuracies are established. Finally, a selection of all possible assembly orders is investigated to conclude that active alignment of the fibre and GRIN lens is preferred.

2.1. Optical path

The optical path of an endoscopic system is shown in Figure 2.1. The light comes from a laser source, travels through a fibre into a GRIN lens and is reflected by a prism.

The quality of the optical path is usually determined by the lateral and axial resolution, and working distance (WD). An image is required to measure the lateral and axial resolution. The lateral resolution is related to the beam diameter (BD), which can be measured in the optical system. In Figure 2.1 the BD and WD are defined for assembling a fibre, GRIN lens and prism. These parameters are influenced by the (mis)alignment of all three elements.

To determine the influence of possible misalignments, we assume that the fibre and GRIN lens are perfect cylinders and that rotations around the z-axis have no influence. This rotation also does not influence the prism, as we assume a perfectly flat reflection surface of the prism. This means that five other misalignments are possible for all parts: two rotations (R_x and R_y), and three translations (Δx, Δy, and Δz). However, these misalignments are linked to each other, for example, a translation of the fibre of $+\Delta x$ is the same as a translation of the GRIN lens of $-\Delta x$. Therefore, the misalignments can be summarized into three parameters, the separation distance, the concentricity (the coincidence of centres) and the collinearity (no angle between the principal axes). To evaluate the influence of these parameters on the complete optical path an overview is made, shown in Table 2.1. We first assume a

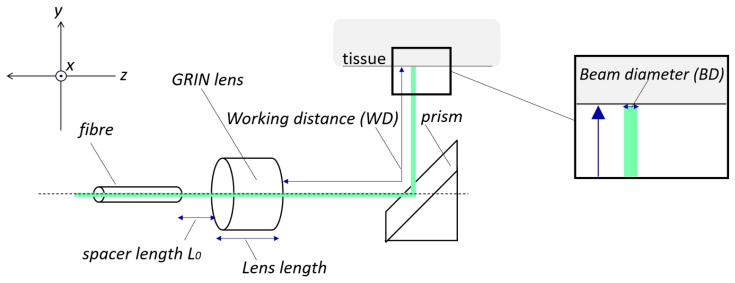

Figure 2.1: Representation of the ideal optical path. The working distance (WD) is defined as the distance from the GRIN lens to the tissue. The beam diameter (BD) is defined as the smallest BD which is always measured at the WD.

	WD	BD	SNR
Misaligned prism			
δx	-	-	-
δy	+	+	-
δz	+	+	-
R_x	+	-	+
R_y	-	-	+
Misaligned GRIN			
δx	+	+	+
δy	+	+	+
δz	+	+	-
R_x	-	+	-
R_y	+	+	-

Table 2.1: Influence of misalignments on beam diameter (BD), working distance (WD) and signal-to-noise ratio (SNR). + indicates the influence of the misalignment, - indicates no influence of the misalignment or an insignificant influence.

perfect alignment of the fibre and GRIN lens and a misalignment of the prism. If the prism is not placed concentrically ($\delta x, \delta y$), this has no effect as long as it is in the range of $40\mu m$ as the BD maximum is about $120\mu m$ and the prism width is not smaller than $200\mu m$ in all analyzed prototypes. However, because of the angled surface, a translation in the y-direction (δy) will also cause a change in separation distance (δz). When the separation distance changes, the prism is out of focus and a larger BD is measured. A change of collinearity (R_x, R_y) will cause the beam to arrive at a different location in the tissue and the signal to reflect on a different spot in the endoscope causing a loss of signal, worsening the SNR. The angularity caused by R_x also causes a changed WD, as the light does not travel along the shortest path to the tissue.

Now, we assume a set location for the prism, based on a theoretical optimum. The misalignments of the fibre or GRIN lens result in the same aberrations, and are therefore not treated separately. Concentricity errors ($\delta x, \delta y$ between the fibre and GRIN lens cause an off-centring of the beam. For this misalignment, [15] shows by ray tracing techniques that the beam leaving the GRIN lens will be angled to the optical axis, causing a loss in the SNR for the same reason as when the prism is angled. Tomlinson [15] concludes that decentring of the fibre does not influence the minimum spot size. However, in this research, the lens length (determining the pitch of the GRIN lens) is changed accordingly with the decentring. This means that not changing the lens will cause a changed BD, which agrees with [4].

Then, if the separation distance (δz) of the fibre and GRIN lens changes, a change in the WD and BD is visible. This parameter influences the WD and BD of which only one can be optimized according to Jung et al. [9]. An analytical analysis and extensive explanation of the influence of this parameter for various materials for optical coherence tomography (OCT) is given by [9] and [17]. An error in this parameter will cause a shift in the WD and BD, improving one parameter while the other one worsens. However, when the WD changes and the prism is not shifted accordingly, the prism will cause an out-of-focus beam at the tissue and a larger BD will be measured. When a tilt between these parts is measured, an increase in the spot size appears. This means the BD is larger and the lateral resolution is decreased [4]. Also, a lateral shift of the beam appears, which is no problem in the x-direction, but due to the angled surface of the prism, it causes a change in the WD when shifted in the y-direction.

It is most important to optimize the SNR, as the BD and WD can never both be optimized. Only two parameters in the misalignment of every part influence the SNR. The misalignment of the prism has less influence on the WD and BD than the misalignment of the fibre or GRIN lens. This analysis contributes to the decision of active alignment of the fibre and GRIN lens.

2.2. Required alignment accuracies

Through a thorough analysis of multiple factors, the alignment of the fibre and GRIN lens was found to be the most important. This paragraph will thus focus on this step and exclude the prism. Based on the influences of misalignments established in section 2.1 we determine the necessary alignment

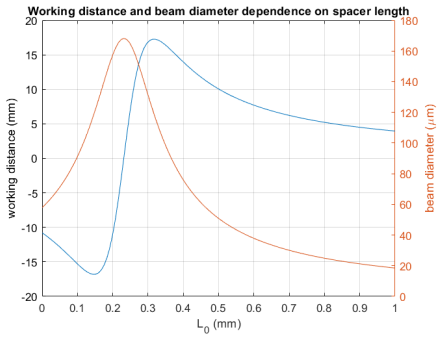

Figure 2.2: Dependence of working distance (WD) and beam diameter (BD) on the spacer length (L_0).

Parameter	Required accuracy
δx	$\pm 3\mu m$
δy	$\pm 3\mu m$
δz	$\pm 5\mu m$
R_x	$\pm 0.23^o$
R_y	$\pm 0.23^o$

Table 2.2: Required alignment accuracies

accuracies of the fibre and GRIN lens. The selection is based on subjectively interpreted literature because no research exists on aligning solely these two parts. The diverse experimental setups lead to a varied definition of the alignment accuracies. The required alignment accuracies are summarized in Table 2.2. Each parameter is individually analyzed, but an error in dx and dy leads to an augmented cumulative error. This is considered during the process, but because misalignments of these parameters are separately visible, their accuracies are also separated.

For concentricity accuracy, we look at the research of [15]. The calculations are done for off-axis alignments up to $0.5mm$ but for a decentring of $0.3mm$ the spot size approximately doubles. This is extremely unwanted and therefore only$1/100^{th}$ of this decentring will be allowed which results in a dy of $3\mu m$ reported in Table 2.2. For the accuracy of the collinearity, the research of [4] is consulted. Although this research does not analyse endoscopes and the test setup includes extra optical elements, it shows the effect of fibre and GRIN lens alignment. In the research a relative tilt of $4mrad$ causes an increase of the spot size from $1.6\mu m$ with about $0.1\mu m$ and the intensity drops about 10% [4]. With more tilt, both parameters increase significantly faster. For example for a tilt of $8mrad$, the spot size increases with more than $0.3\mu m$ and the intensity drops to about 65% of the value for no tilt. Therefore a maximum tilt of about $4mrad$ (~ 0.23 degrees) has to be achieved. These goals are estimations, based on the rare research that was available, and feasibility is not yet considered.

Finally, the separation distance between the fibre and the GRIN lens is investigated. As this is a design parameter, the optimum can be different for every prototype. The relation between the BD and WD as a result of the separation distance L_0 is shown in Figure 2.2. This calculation is performed using the method from [13], where a no-core fibre is added to fill the space between the fibre and GRIN lens. This only changes the refractive index of the separation distance, making it a valid method. When the input beam width changes, the graph changes a lot. This value depends on the laser source (wavelength and power), which can be varied during experiments. Therefore, it is unlikely to validate the theoretical values experimentally. However, for early-stage endoscopic prototypes, repeatability is important. This means a similar result in different tests is important. [6] and [7] by the same researchers, mention a separation distance precision of $2\mu m$. Preferably all prototypes meet this standard even though these assemblies are significantly smaller than the probes this thesis focuses on. While optical imperfections spread out the beam waist, minor deviations in separation have minimal impact on results as shown in Figure 2.2. Thus, the required precision is relaxed to $5\mu m$. This parameter is the only one for which the exact spot (accuracy) is less important than its repeatability (precision).

Precision parameter	Dimensions and tolerances
Separation distance	
Length fibre	-
Length GRIN lens	$3.93mm \pm 0.20mm$
Concentricity	
Diameter fibre	$125\mu m \pm 1\mu m$
Core centring fibre	$\leq 1\mu m$
Diameter GRIN lens	$1.80mm + 0.00/-0.01mm$

Table 2.3: Dimensions and manufacturing tolerances of fibre and GRIN lens (Fibre: Thorlabs SM600; GRIN lens: Edmund Optics 64-538)

2.3. Manufacturing tolerances on parts

For aligning parts during assembly it is essential to consider the manufacturing tolerances of the used parts. These tolerances may vary between manufacturers. These inaccuracies will however affect the assembly process, thus we consider in this work the manufacturing tolerances of the parts ordered (Table 2.3). The housing is excluded from this examination because this part varies greatly among the prototypes and tolerances cannot be presumed. The manufacturing tolerances of the optical elements used in this research are shown in Table 2.3, but it is important to notice that other prototypes will have different preconditions. Also, the collinearity of the parts is not included because this parameter is not influenced by the manufacturing tolerances. The fibre length and its tolerances are not specified, as this dimension does not affect the assembly process in the probe. The required accuracies from Table 2.2 and the manufacturing tolerance from Table 2.3 show an evident imbalance, requiring a study to overcome the separation.

2.4. Assembly orders

The order in which the optical elements of an endoscope can be assembled is finite. The selection process for the best assembly order is primarily characterized by the feasibility of minimizing errors in the optical path. The bonding of the parts is a crucial step in the assembly process but is out of the scope of this research. Therefore, only the assembly order and aligning method are researched.

2.4.1. All assembly orders

We chose to present the problem of the order of assembly as a problem of four parts, the fibre, GRIN lens, prism, and housing. There are two ways to assemble four parts. The first one is sequentially joining all separate parts, resulting in 4! = 24 possible assembly orders. However, there are identical orders because the order of the first two parts in the assembly is irrelevant. Therefore, only 12 distinct assembly orders exist for the four presented parts. All possibilities are shown in Appendix A. The second way to assemble four parts is to use sub-assemblies. Two parts are joined, and the remaining two parts also form a sub-assembly. These two sub-assemblies are joined together into the final assembly. Because the first sub-assembly immediately determines the second sub-assembly, only three distinct assembly orders are possible, generating 12 + 3 = 15 unique assembly orders. In five options the fibre and prism are assembled passively first and the GRIN lens is placed between these two parts. This is very prone to errors because a misalignment of either the fibre or the prism can not be accounted for by the alignment of the GRIN lens. Therefore, these five options are discarded. As a result, there are 15 - 5 = 10 valid unique assembly orders.

2.4.2. Selection of Preferred Assembly Order

An active alignment procedure ensures greater accuracy than a passive alignment method. Given that the tolerances found in section 2.3 were in the few micrometre range, an active alignment procedure is needed for a repeatable process. Because actively adjusting at least five degrees of freedom for multiple elements is too time-consuming and costly we only consider introducing one active alignment step.

For all ten assembly orders, three steps can be done actively. However, actively aligning the optical elements to the housing structure is impossible without using additional optical elements which is

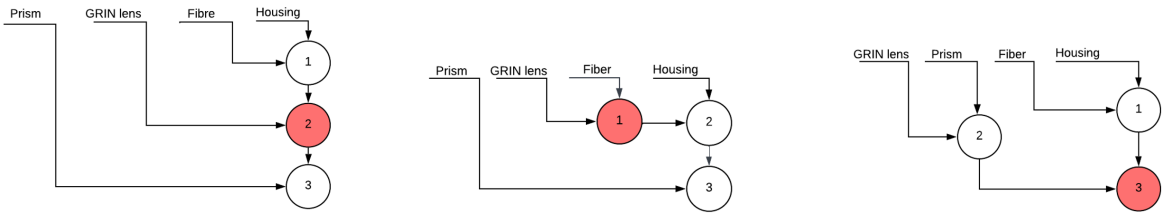

(a) Assembly order A (b) Assembly order B (c) Assembly order C

Figure 2.3: Three best alignment orders considered, the red circle indicates the step where active alignment is applied.

unwanted. Therefore, assembling the housing with optical components is never done actively, leaving only two steps available for active alignment in every process, which can be generalized in two alignment challenges. The first is to align the fibre and GRIN lens to create the best beam. The second option is to align the prism to the optical axis of the fibre and GRIN lens. Only one of these challenges is chosen to be actively aligned. For the alignment of the prism to the GRIN lens and thus the optical axis, it is relevant to notice that the fibre and GRIN lens should already be present to use the light source for active alignment. Instead of analysing all twenty possible assembly orders including the active alignment procedure, a choice is firstly made between actively aligning the fibre and GRIN lens or the GRIN lens and prism. This choice is based on the analysis in section 2.1.

The misalignment of the fibre and GRIN lens will introduce errors that are hardly reversible by precise alignment of the prism (see section 2.1). Locating the prism at the correct position concerning an unknown optical axis is very challenging as the housing structure limits its space. Also, the alignment of the fibre and GRIN defines the maximum achievable WD and minimum achievable BD, and can not be improved by the prism anymore. For example, when the fibre and GRIN lens are aligned under an angle, the beam profile changes and causes a distorted focal spot. A distorted focal spot with an asymmetric wavefront will cause a reduction of the SNR. This can be enhanced by image processing, but this is very time-consuming because every prototype will have different distortions, and no automation of this process is possible. Therefore, the alignment of the fibre and GRIN lens is prioritized over the alignment of the GRIN lens and prism.

This decision limits the options for the various assembly orders including an active alignment method. Because of this, some of the resulting assembly orders show an extremely similar problem. An extensive explanation of this similarity is added in Appendix A. Ease of part handling also influences the choice of a particular assembly sequence. It is preferred to move the GRIN lens instead of the fibre, leaving only three possible alignment orders for the parts of the optical system of an endoscopic prototype, these are shown in Figure 2.3.

Finally, the decision is between aligning the fibre and GRIN lens inside the housing, or outside the housing and relocating it into the housing. Although fixing the elements is not included in this selection process, it is essential to recognize that the fibre and GRIN lens are not necessarily fixed together after

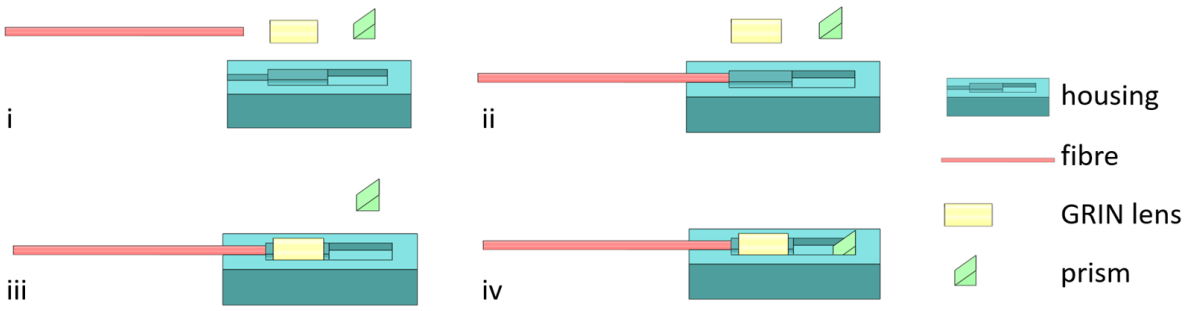

Figure 2.4: The selected assembly order: (i) all parts to assemble (ii) fibre placement (iii) GRIN lens placement by active alignment (iv) prism placement

the first assembly step outside the housing. This creates extra challenges concerning the relocation of this sub-assembly. Concluding, because relocation introduces extra handling steps and may introduce new errors and there is no clear advantage, assembly outside the housing is discarded. This leaves assembly order A from Figure 2.3 order as the best one to continue with. The consecutive steps of the process are shown in Figure 2.4.

3

Calibration and Alignment Procedure

A test setup is created to validate the assembly order's working principle. First, an overview of the complete assembly procedure is given. In the following paragraphs, the main steps of the procedure are discussed in depth leading to the necessary components for the setup.

3.1. Procedure overview

The complete fibre and GRIN lens alignment procedure consists of four main steps.

- Clamp the fibre to the housing
- Align the fibre and beam profiler
- Calibrate the fibre and its stages, and the beam profiler and its stages
- Align fibre and GRIN lens

The initial step involves securely clamping the fibre to the housing to secure the component. Due to the fibre's vulnerability, this step is not performed for every measurement. In a complete prototype, the fibre would be glued to the housing, but then the fibre would not be reusable as is necessary for this experiment. The complete setup is shown in Figure 3.1 and consists of three entities of multiple stages. All stages in this setup are numbered and an overview of their specifications is shown in Table 3.1.

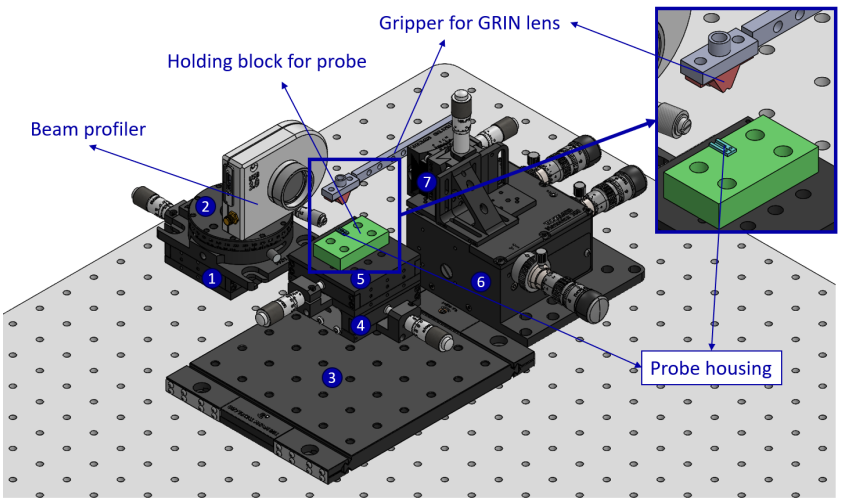

Figure 3.1: Overview of the setup: (1), (4) and (5) linear translation stages; (2) rotation stage; (3) large range translation stage; (6) precision translation stage; (7) double rotation stage

Stage nr	Range of motion	Resolution
(1) (4) (5)	25 mm	10 μm
(2)	360^o	5 arcmin (0.083^o)
(3)	50 mm	None
(6)	4 mm	1 μm
(7)	5^o/10 ^{o}	10 arcmin (0.167^o)

Table 3.1: Range of motion and resolution of all stages used in the setup

3.2. Aligning the fibre and the beam profiler

To align the fibre and the beam profiler, both components need certain degrees of freedom. The beam profiler is therefore mounted on a translation stage (1) along the z-axis to allow imaging multiple planes of the beam and a rotation stage (2) for alignment with the beam. The fibre clamped to the housing is placed on three stages, a large-range translation stage (3) along the z-axis and two translation stages (4) (5) along the x- and z-axis. Also, during the alignment of the fibre and beam profiler, filters and lenses are incorporated into the beam profiler setup. This adjustment is necessary as the light emitted from the fibre diverges too much, limiting the accuracy of the beam image. The measurements validating this adjustment are detailed in Appendix B. This adjustment is also the reason for the coarse and fine alignment of the fibre in the z-direction. When the lenses are removed, the fibre should be brought into close range of the beam profiler.

Three parameters are subject to optimization to ascertain the angle between the fibre and the beam profiler: the symmetry of the beam profile along the y-axis, the centring of the beam profile along the x-axis, and the orientation angle of the principal axes of the beam profile. Symmetry indicates the angular deviation between the fibre and beam profiler when the fibre aligns precisely with the lens centre. This principle is shown in Figure 3.2 and an example is shown in Figure 3.3. When the fibre is exactly at the centre of the lenses, the beam's centre coincides with the centre of the x-axis. Lastly, the orientation of the principal axes validates the first two parameters.

A coarse alignment is done by looking at the beam profile and finding an optimum. Measurements are taken around this optimum within a range of 2 degrees with a change of 25 arcmin (0.417 deg) for verification, leading to an optimal alignment with a precision of 25 arcmin. See chapter 4 for the results of these measurements. Other methods of aligning the fibre and beam profiler were researched but proved impossible. These methods and results are shown in Appendix B.

3.3. Calibrating the fibre and the beam profiler

The fibre has a different coordinate system than the stages it is mounted on. Also, the beam profiler has a separate coordinate system from its stages. The effect of this is shown in Figure 3.4. When the fibre is moved in the z-direction, a parasitic translation occurs in the x- and y-direction. Therefore

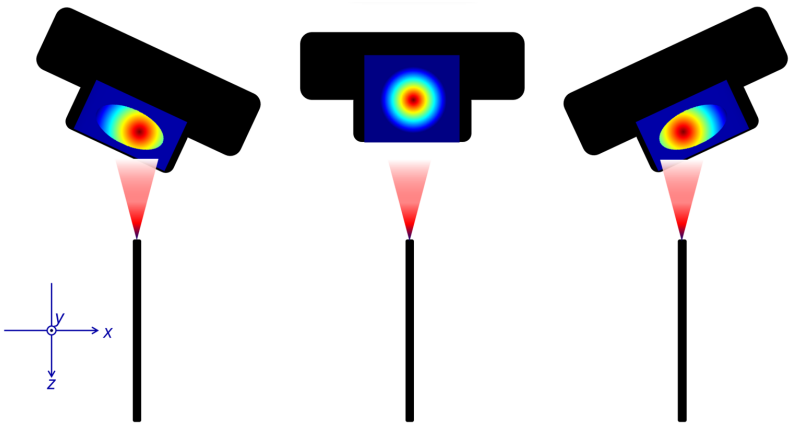

Figure 3.2: This image shows a top view of aligning the fibre and beam profiler. The skewing in the beam profiles is made visible.

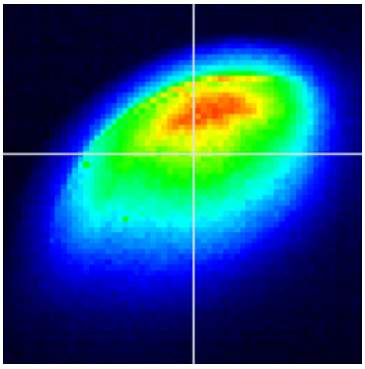

(a) Beam profile of extremely rotated fibre with respect to the beam profiler

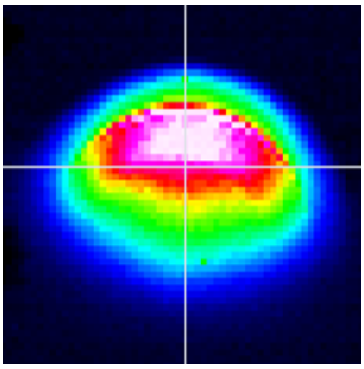

(b) Beam profile of orthogonal fibre in one direction with respect to the beam profiler.

Figure 3.3: Beam profile when a light source is misaligned (extremely angled) to a beam profiler and when it is orthogonal.

calibration of the fibre and beam profiler is essential. The fibre's stages are moved $100\mu m$ and the position of the beam's centre is measured. This shows the change introduced by the stage. The same is done for moving the beam profiler.

Because these calibrations are only done with translation stages, the errors are expected to be linear, and by inter- and extrapolation, the erroneous translations can be calculated. For example, if the fibre is translated in $100\mu m$ in the z-direction, the x-coordinate changes $5\mu m$, and the y-coordinate $2\mu m$. If a translation of $1000\mu m$ of the fibre in the z-direction is necessary, the system calibration yields then that the optical axis is changed $50\mu m$ in the x-direction and $20\mu m$ in the y-direction with respect to the optical axis of the beam profiler.

3.4. Aligning the fibre and the GRIN lens

To align the fibre and GRIN lens, the GRIN lens is picked up by a vacuum gripper and placed in front of the fibre. The coarse alignment involves adjusting the fibre's position, resulting in a new optical axis. Using the calibration the new optical axis with respect to the beam profiler can be calculated as explained in section 3.2. The fine alignment is performed by positioning the GRIN lens, using a precision translation stage (6) for all three translations with a rotation stage (7) mounted on top for the rotations around the x and y axes.

Then, the GRIN lens is aligned using the same parameters and methods as for the alignment of the fibre and beam profiler. However, some extra factors need to be considered.

It is essential to understand the consequences of displacements of the GRIN lens to align the fibre and GRIN lens. Therefore, the lateral displacements $(\delta x, \delta y)$ are investigated separately from the

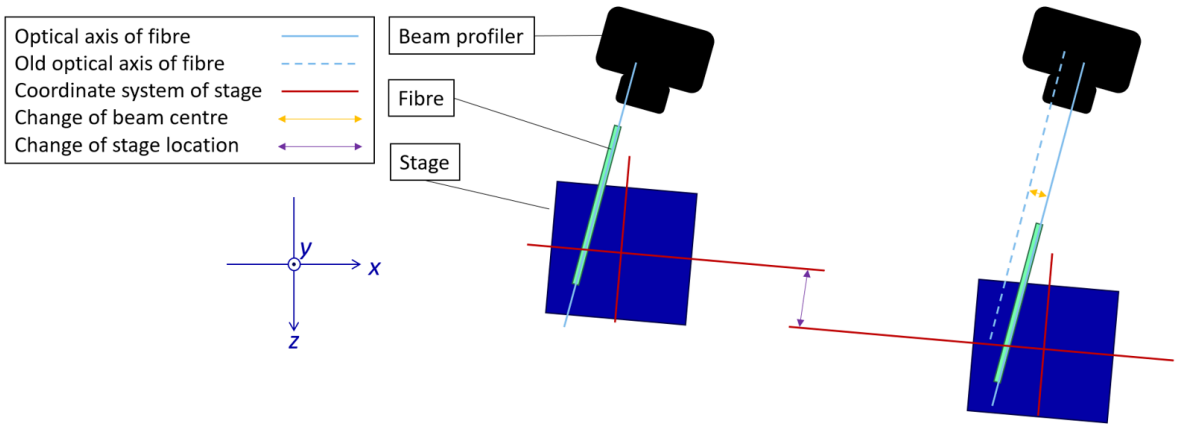

Figure 3.4: Effect of different coordinate systems. A translation along one axis results in an erroneous translation along another axis.

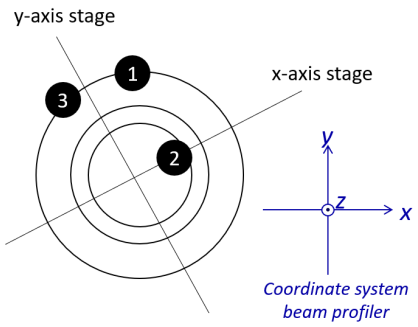

Figure 3.5: The thin circles represent different refractive indices of the GRIN lens, and the numbered black circles represent beam positions. This shows the challenge of having two perpendicular axes to align two circular objects.

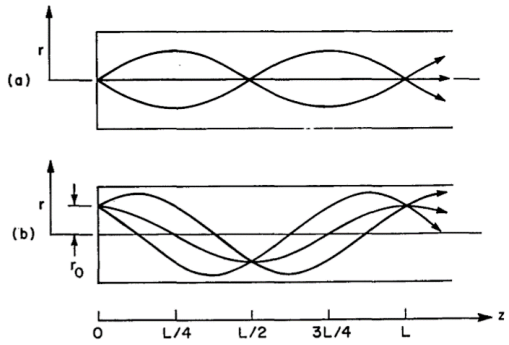

Figure 3.6: Cross sections of GRIN rods, showing ray paths for an object point (a) on-axis and (b) off-axis [15]

rotations. The displacements are performed by one stage with such high precision we can assume the motion is perpendicular.

The lateral displacements of the GRIN lens are not in the same coordinate system as the fibre. Therefore, if the GRIN lens is repositioned with a distance of δx, it results in a new position of the beam profile over a distance δy and δx. Apart from this, an extra, unpredictable change in the position of the beam profile is visible. This change is caused by the circularity of the components and the limited ability of the setup to move along two perpendicular axes. In Figure 3.5 an example is visible. The circles represent different refractive indexes of the GRIN lens, and the numbered circles represent the beam's location. The first position can be represented by an x- and y-coordinate (at the beam profiler's coordinate system or the GRIN lens' coordinate system), or by an angle and radius in the GRIN lens' coordinate system. The goal is to reach concentricity, thus a zero radius, for alignment, but only the x- and y-coordinates can be adjusted. Adjusting the y-coordinate to get to position 2 changes the angle and radius of the detected beam, but does not optimize them. When the beam changes to position 3, the radius does not change, not changing the optimization of the alignment. Important to notice is that this change in position causes the beam profile's centre to change due to the angled beam leaving the GRIN lens. This angularity also creates a skewed image. The ray propagation in a GRIN lens is shown in Figure 3.6. The angular positioning of the GRIN lens needed to reach colinearity will also cause translations in the position of the GRIN lens as shown in Figure 3.7. Because of the factors explained above, determining the optimal alignment is challenging. Also, a purely angled GRIN lens only causes a shift in the beam, not a distortion of the wavefront or an angled beam causing a lower SNR. Therefore, the method for alignment is mostly based on lateral alignment to reach the concentricity of the fibre and GRIN lens. Because any angular adjustment will cause a translation too, as shown in Figure 3.7 these steps are repeated several times to find a more optimal result. The results of aligning the fibre and GRIN lens are presented in chapter 4.

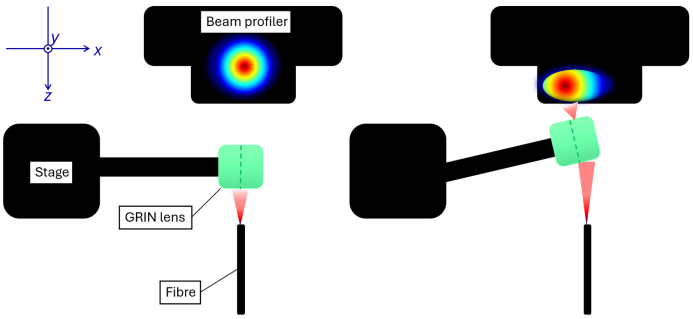

Figure 3.7: The left image shows an ideal position and the right image shows the effect of rotation on the position of the GRIN lens. A parasitic translation is introduced.

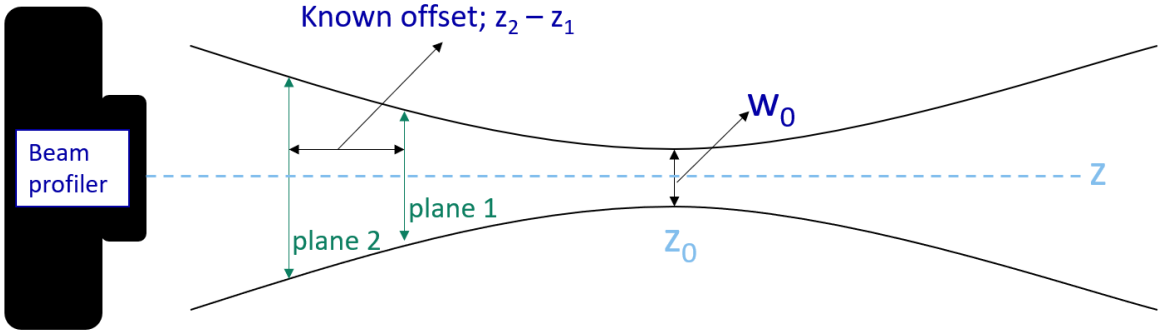

Figure 3.8: Basic Gaussian beam showing the measured parameters for the calculations

With the current setup, the separation distance between the fibre and GRIN lens is estimated by calculating the beam diameter (BD) at the focal spot. By imaging multiple planes of the output beam as shown in Figure 3.8, the BD of the image changes and the BD of the focal spot can be calculated using Equation 3.1. The separation distance can be determined using the relation between the BD and separation distance in Figure 2.2. For the separation distance, the repeatability is the most important. Therefore, five consecutive measurements are performed to determine the accuracy of the placement. The separation distance is directly linked to the BD, and therefore the goal is to get the same BD in all five measurements, with the same intensity profile.

$$w(w_0, z) = w_0 * \sqrt{1 + \left(\frac{z}{z_r(w_0)}\right)^2} \quad \text{with} \quad z_r(w_0) = \frac{\pi * w_0^2 * n}{\lambda} \tag{3.1}$$

Known parameters:
$w(w_0, z)$ = BD at firstly measured plane $[\mu m]$
n = refraction index of medium (air)
λ = wavelength $[\mu m]$

Calculated parameters:
w_0 = BD at focal spot $[\mu m]$
z = separation distance between fibre and GRIN lens $[\mu m]$

4

Results

The results of the measurements are shown in this chapter. First, the system is analysed without aligning any components to validate the system's working principle and calibrate it. Then, the results of the alignment of the fibre and beam profiler are presented, and finally, the results from the alignment of the fibre and GRIN lens are stated.

4.1. Setup validation and sensitivity analysis

We analyse the system sensitivity by measuring the beam's centre location and the beam diameter (BD) of the light that comes from the fibre and falls onto the beam profiler. To improve the sensitivity, lenses are added in front of the beam profiler to focus the light. The results of a one-minute measurement with a measurement interval of 1 second are shown in Figure 4.1 and in Table 4.1. These results show that the beam focusing creates a more stable image and a better sensitivity, especially for the BD. The BD is measured along the principle axis, and the effective diameter is calculated as the average of these two. The centre's standard deviation is almost reduced by 50%. The diameters from Table 4.1 indicate that the beam profile is oval. This is because the fibre and beam profiler are misaligned and can not be adjusted in every degree of freedom. Both can not be rotated around their x-axis, creating a stretched image along the y-axis.

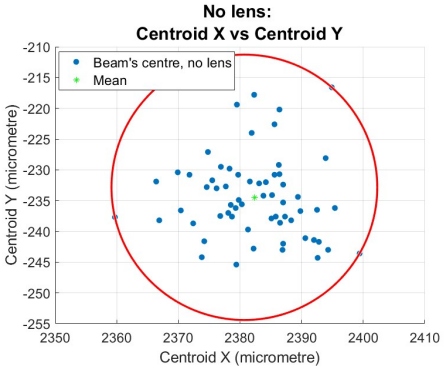

(a) Scatter plot of the beam's centre measurement every second for one minute with only the fibre and beam profiler present

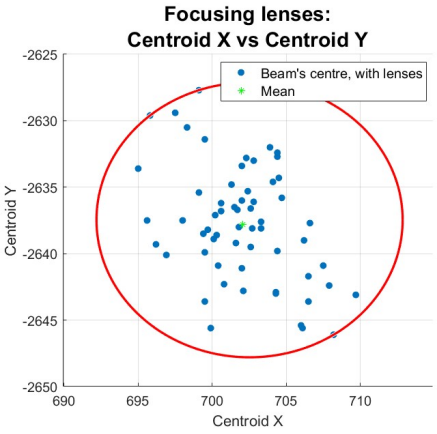

(b) Scatter plot of the beam's centre measurement every second for one minute with the fibre and beam profiler with focusing lenses present

Figure 4.1: Scatter plots showing the difference between a setup using focusing lenses and a setup without lenses.

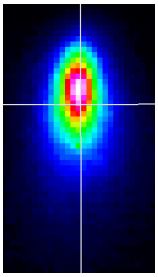

Figure 4.2: Initial coarse alignment of fibre and BP

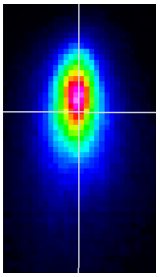

Figure 4.3: Final alignment of fibre and BP

	Initial BP	Final BP
Diameter x (μm)	71.5	71.5
Diameter y (μm)	33	38.5
Orientation (deg)	0.21	-0.07
Centre x (μm)	0.23	-0.01
Centre y (μm)	347.88	348.37
Saturation level (%)	92.53	78.63

Table 4.2: Comparison between the initial beam profile and the final result of the beam profile after aligning the fibre and beam profiler

4.2. Angular alignment of the fibre and beam profiler

Results obtained from the alignment process of the fibre and beam profiler are represented here, validating the orthogonality. Initially, a beam profile of the coarse alignment is presented in Figure 4.2, showing the initial alignment point found by trial and error based on visual inspection. In Figure 4.3 the final result of the best alignment is presented and Table 4.2 shows the most important variables of both images for comparison. This comparison shows that the initial alignment is extremely close to the final result. Figure 4.4 illustrates ten beam profiles captured near the coarse alignment with steps of 25 arcminutes (0.4167^O). These results show that there is a clear difference. Figure 4.5 contains a plot of the centroid position on the y-axis and the orientation angle on the x-axis, contributing to selecting the best measurement and validating the precision obtained in the alignment process. Visually, the best measurement from Figure 4.4 is image 4 or 5, because the body is the most symmetric (only symmetric along the y-axis). From Figure 4.5, measurement 5 has the best orientation and location. Therefore the beam profiler is returned to the position of measurement 5. Figure 4.3 depicts an image taken after returning to this position. When comparing the optimal orientation (in this instance, measurement 5) with the best-obtained orientation after measuring, the angle fluctuates between -0.2^O and 0.4^O, while the centre varies between $-0.3\mu m$ and $0.4\mu m$. Although these variations extend to neighbouring measurements (such as measurements 4 or 6), they are never simultaneously as significant and consistently remain closer to the optimal measurement.

4.3. Calibration of fibre and beam profiler

The measurements of a calibration step as explained in chapter 3 are shown in Figure 4.6 and Figure 4.7 for the fibre and in Figure 4.8 for the beam profiler. The stages are translated over a distance of $100\mu m$ for each measurement. This shows a linear correlation as expected, except for the x-translation of the fibre. This is also expected as the distance between the fibre and beam profiler is not changing and thus the y-position of the beam remains unchanged. Using the ratio of change between the stages and the beam's centre, the centre of the beam for different positions can be calculated based on the position of the stages. These calibration steps must be repeated for every change in the setup or new fibre position.

4.4. Aligning the fibre and GRIN lens

The three different variables of the fibre and GRIN lens alignment (concentricity, colinearity and separation distance) are evaluated separately to determine the sensitivity. The aim is to reach the best possible alignment position and test the repeatability.

4.4.1. Sensitivity of fibre-GRIN lens alignment

Measurement:	**Centre x** $\pm\sigma$	**Centre y** $\pm\sigma$	**Diameter x** $\pm\sigma$	**Diameter y** $\pm\sigma$	**Effective diameter** $\pm\sigma$
No lenses	2382.4 ±7.9	-234.5 ±6.6	1856.9 ±162.4	2274.7 ±228.0	2065.8 ±151.5
With lenses	702.1 ±3.3	-2637.8 ±4.3	1316.2 ±73.2	1200.8 ±109.6	1258.5 ±60.5

Table 4.1: Mean values of one-minute measurements, data is stored every second. All units are μm

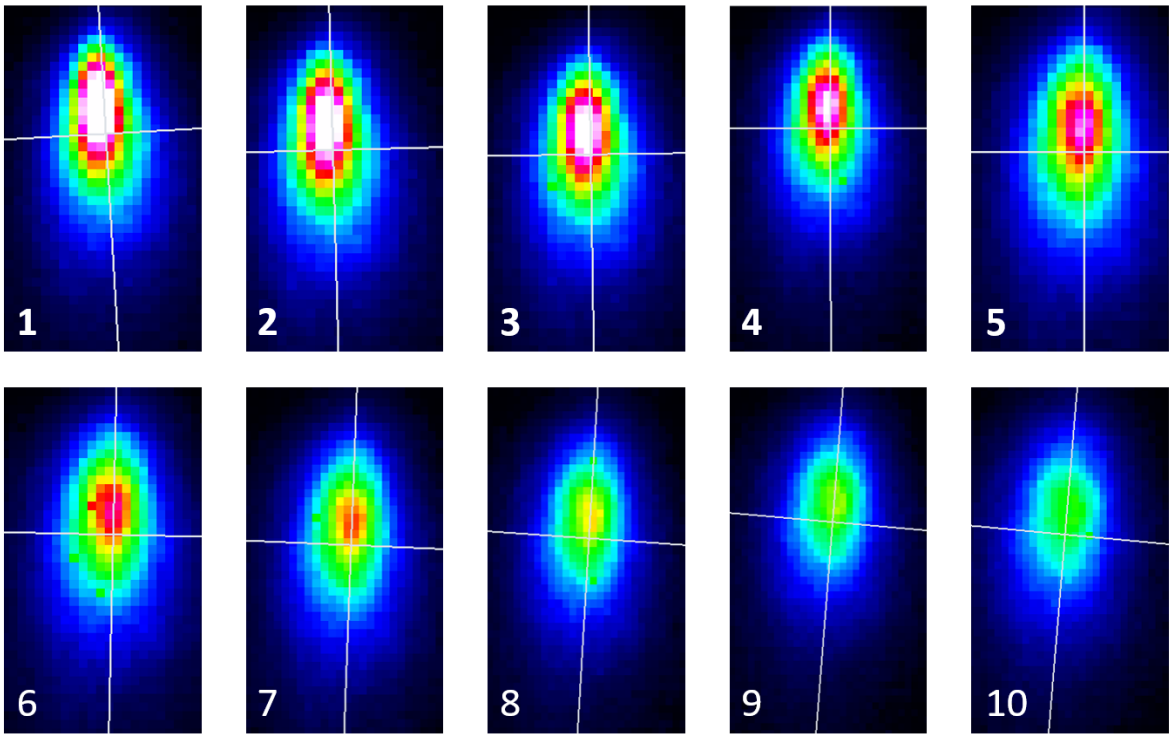

Figure 4.4: Complete set of measurements determining the optimal orthogonal alignment of the fibre and beam profiler/

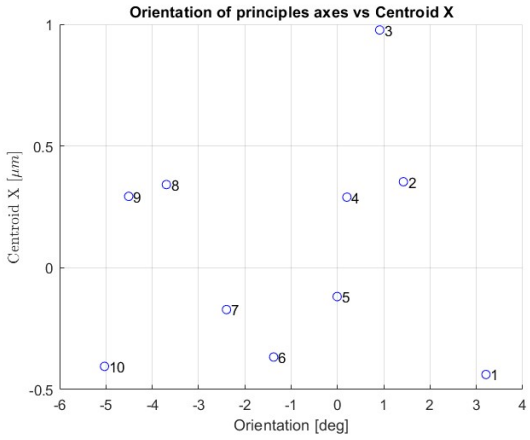

Figure 4.5: Scatter plot to determine the best position for orthogonality of the fibre and BP

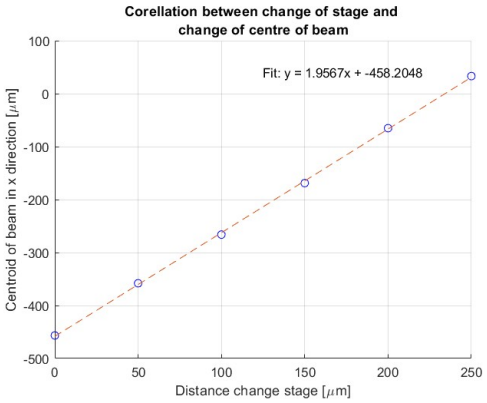

(a) Relation between the change in x-direction of the fibre's stage and the beam's centre in x-direction

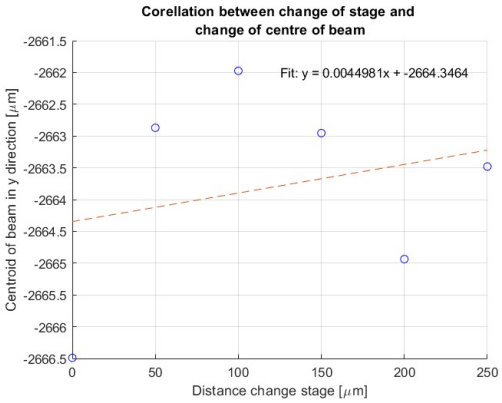

(b) Relation between the change in x-direction of the fibre's stage and the beam's centre in y-direction

Figure 4.6: Plots for calibration measurements of fibre in x-direction

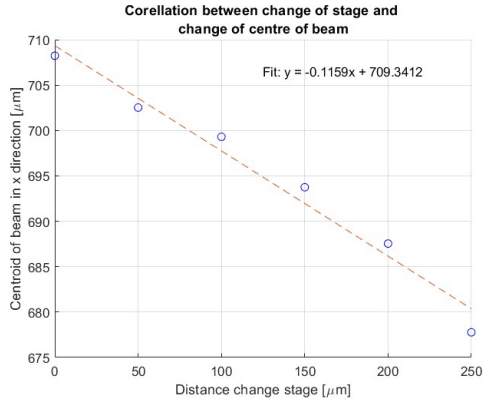

(a) Relation between the change in z-direction of the fibre's stage and the beam's centre in x-direction

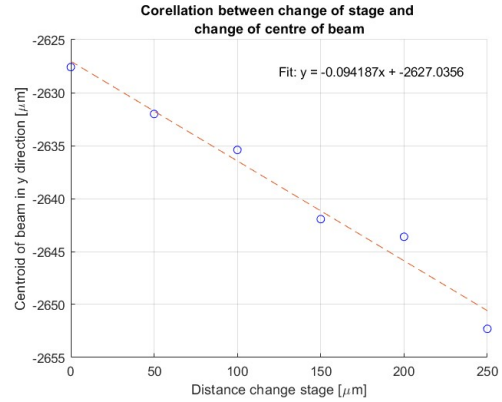

(b) Relation between the change in z-direction of the fibre's stage and the beam's centre in y-direction

Figure 4.7: Plots for calibration measurements of fibre in z-direction

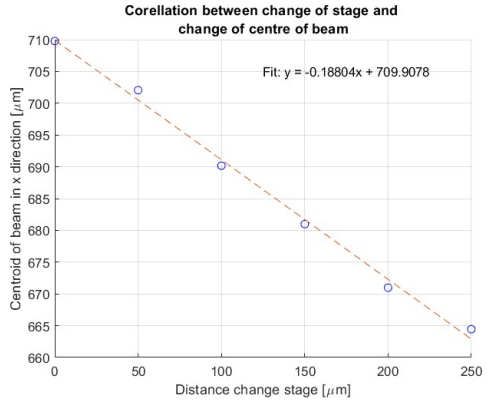

(a) Relation between the change in z-direction of the beam profiler's stage and the beam's centre in x-direction

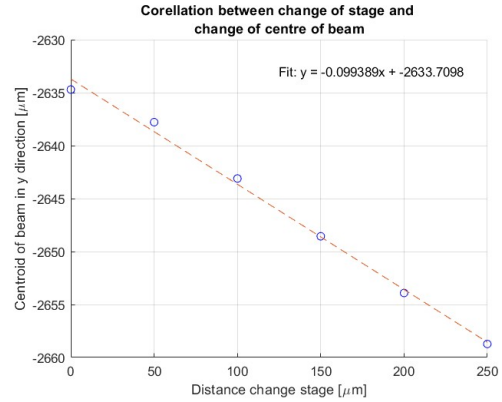

(b) Relation between the change in z-direction of the beam profiler's stage and the beam's centre in y-direction

Figure 4.8: Plots for calibration measurements of beam profiler in z-direction

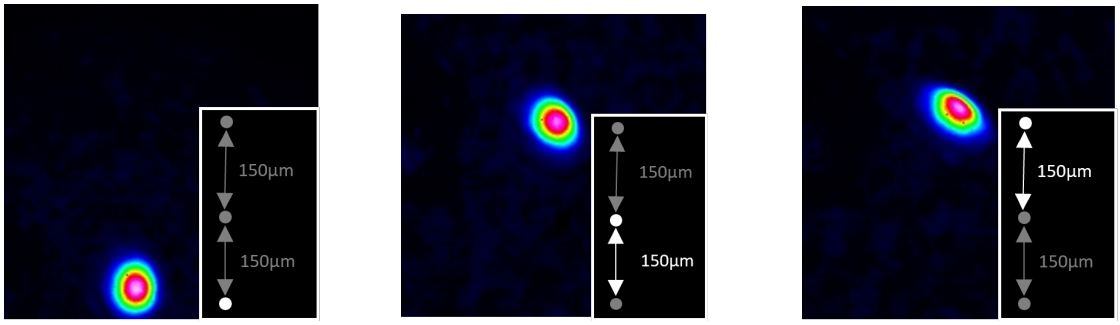

(a) Least possible skewing

(b) Slightly skewed image after $150\mu m$ change of GRIN position

(c) Largly skewed image after another $150\mu m$ change of GRIN position (total change from starting point is $300\mu m$

Figure 4.9: Three beam profiles at three different positions (change of 150 μm in y-direction per image) showing the skewing of the beam profiles

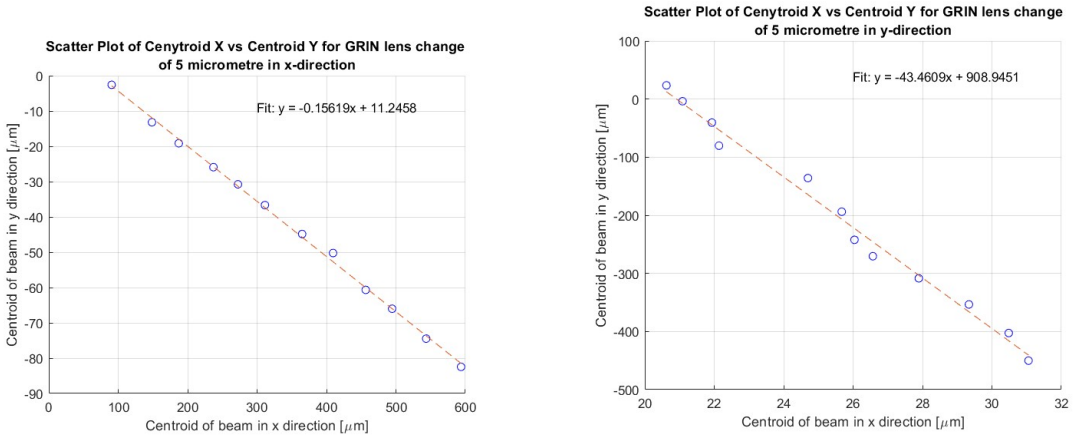

(a) Plot of beam centre after lateral displacement of the GRIN lens in x-direction with steps of $5\mu m$

(b) Plot of beam centre after lateral displacement of the GRIN lens in y-direction with steps of $5\mu m$

Figure 4.10: Plots of beam centre after lateral displacements of the GRIN lens

Concentricity: Lateral displacement of the GRIN lens

To position the GRIN lens, two lateral displacements are possible. As explained in section 3.4 a lateral change will not always change the shape of the beam profile, but it will always change the position of the beam profile. Three measurements are taken to confirm that a lateral change will cause the beam to be at an angle and that a skewed beam profile is visible. The beam profiles collected from these images are visible in Figure 4.9. The skewing in the images indicates that a better position can be reached, but it is only clearly visible after a change of $150\mu m$. Smaller lateral displacements do not show significant skewing visible by the eye, but the beam's location, orientation, and diameter change. Combining all information, an optimization algorithm might display better sensitivity than $150\mu m$.

Figure 4.10 shows the change of the beam centre for every change of $5\mu m$ of the GRIN lens in the x-direction. Figure 4.10a shows that the change of the GRIN lens in one direction causes a change of the beam profile in two directions. The relation also shows that smaller changes in the position of the GRIN lens are also measurable. In Figure 4.10b this is different, the beam only changes a few microns in the x-direction. In Appendix C two additional measurements show the influence of the beam profiler's position and the separation distance of the fibre and GRIN lens on the sensitivity.

Colinearity: Angular displacement of the GRIN lens

The GRIN lens can be rotated around the x- and y-axes. However, these rotations are also causing translations because of the different coordinate systems and the extension of the gripper arm. This requires large counter translations to keep the light falling onto the beam profiler. These results are therefore nearly impossible to process in terms of BD and centre location. The translations are unknown

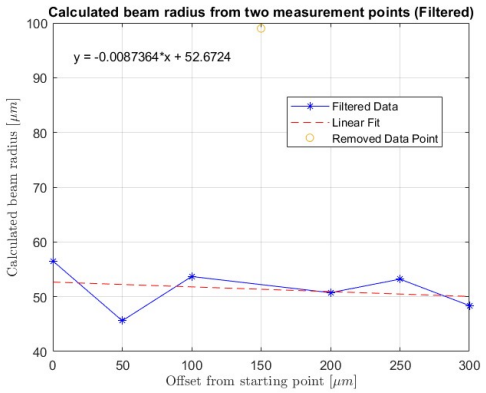

(a) Beam diameter (BD) calculation based on measurements of different planes of the light beam (the beam profiler is moved $50\mu m$ every measurement)

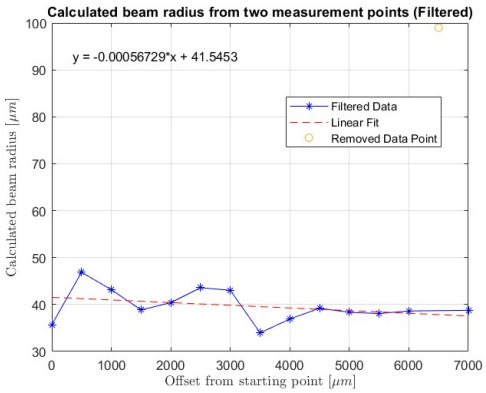

(b) Beam diameter (BD) calculation based on measurements of different relative planes of the light beam (the beam profiler is moved $500\mu m$ every measurement)

Figure 4.11: Calculated beam diameter (BD) for moving the beam profiler in two different measurements with different-sized steps

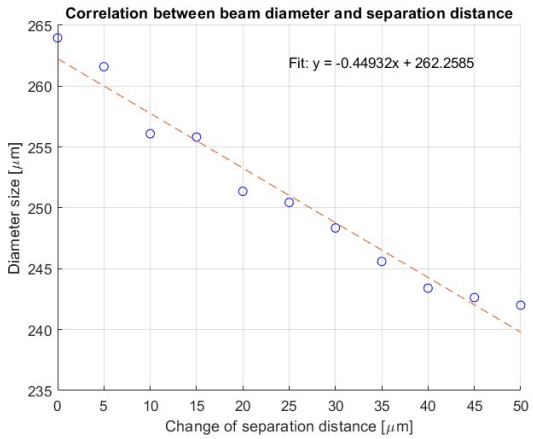

Figure 4.12: Relation between the separation distance and the beam diameter (BD)

and can not be countered. Therefore a pure rotation can not be performed, and the sensitivity cannot be calculated. The complete measurements are shown in Appendix C to show the results of the rotations including the translations.

Separation distance: Distance positioning between fibre and GRIN lens

Changing the separation distance changes two directly measurable variables. The first one is the intensity, which is not used in this research, and the second is the BD. The smallest BD is calculated using the measured BD. Because of the different coordinate systems, the beam's centre also changes. This data can be found in Appendix C. Figure 4.12 shows the correlation between the separation distance and the BD. This image shows that for a change of $10\mu m$ the diameter decreases $\pm 4.5\mu m$. The pixel width of the used beam profiler is $5.5\mu m$. The diameters in Figure 4.12 are the means of the values of the primary axes, averaged over measurements of half a minute. Although this introduces an uncertainty, the sensitivity is sufficient to use the measurements for calculations of the smallest BD and separation distance.

We calculate the BD for two measurements by moving the beam profiler with steps of $50\mu m$ and $500\mu m$. The calculated BD, shown in Figure 4.11 lies within $10\mu m$ for both measurements and is in the range of $50\mu m$, which is expected.

4.4.2. Optimal position of the GRIN lens

A perfect image would look like a circle and be positioned with the centre at the calculated spot. This image is pursued, using the iterative method described in chapter 3. Because the beam profile changes

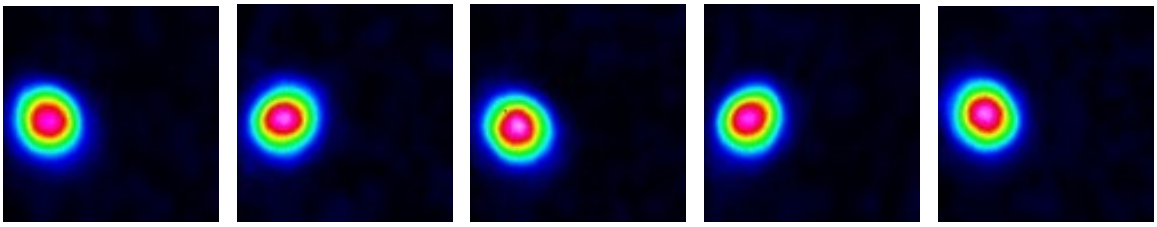

(a) Try 1 for best beam profile (b) Try 2 for best beam profile (c) Try 3 for best beam profile (d) Try 4 for best beam profile (e) Try 5 for best beam profile

Figure 4.13: Five beam profiles, where the first one is found by optimization, and used as a reference for the other four. The goal was to find the same beam profile again, with the same shape, diameter and intensity.

continuously, it is challenging to determine its symmetry and circularity by eye. Therefore, only an estimated guess of an optimal image can be attained with this setup. The best image reached is shown in Figure 4.13a.

Repeatability

A crucial factor in the manufacturing of probe prototypes is the repeatability. To ensure that all prototypes are similar, the placement of the GRIN lens should be the same for every probe, even if the fibre is positioned differently. The GRIN lens is positioned in front of the fibre five times to test whether this is possible with the current setup. The other four images in Figure 4.13 were obtained by optimization and comparison with the first image (Figure 4.13a). It shows the challenges of manual optimization and that visual inspection is insufficient for reaching the same beam profile multiple times. In Table 4.3 the most important parameters for comparison are shown. The results show that although there is a clear difference between the images some important variables are very similar. The first three columns show the diameter along the x- and y-axes and the effective diameter (used as BD) is the mean of these two. These results show that the BD is within $6\mu m$, although the y-diameter varies up to $15\mu m$. In Figure 2.2 it shows the largest change of the BD is around a spacer length of $0.25mm$. A comparison of two data points with a difference of $15\mu m$ in the BP shows that the spacer length is changed with about $40\mu m$ between those points. This means the GRIN lens is positioned with repeatability of $\pm 40\mu m$.

The ellipticity shows that there is still clear variation in the shape of the beam profile, which was already concluded by comparing the images side-by-side. The intensity also varies with about 5%, showing there is a difference in the separation distance of the fibre and GRIN lens.

	Diameter x (μm)	**Diameter y** (μm)	**Effective diameter** (μm)	**Ellipticity (%)**	**Intensity (%)**
M1	114.0	117.0	115.5	96.0	92.8
M2	118.3	123.4	120.8	93.7	88.0
M3	115.1	116.6	115.9	96.6	93.2
M4	119.7	108.9	114.3	91.1	89.4
M5	118.2	117.6	117.9	97.0	91.9

Table 4.3: Results of five measurements trying to get the same beam profile

5

Discussion

The results of chapter 4 indicate that the proposed method of chapter 3 is promising. While the results for sensitivity and repeatability approximate the predefined goals, there remains room for improvement. In Table 5.1 an overview of the goals and reached results is presented for the sensitivity and repeatability of each step in the process. This chapter first discusses the sensitivity of each step, and then the repeatability of each step.

Sensitivity

Firstly, the sensitivity for aligning the fibre and beam profiler is found to be inadequate. While this parameter wasn't explicitly specified, any potential errors in this alignment will add to the errors in aligning the fibre and GRIN lens. Even a slight misalignment in these components can result in a changed measurement outcome of the beam diameter (BD), a critical factor in this study used to determine the separation distance. However, the separation distance between the fibre and GRIN lens is primarily crucial for its repeatability so a precise method with a relatively low accuracy is acceptable. To improve this alignment several alterations to the setup are proposed. The fibre is now only movable in two directions: along the x-axis and the y-axis. The addition of two rotation stages enables precise positioning of the fibre at the correct angle to the beam profiler. This adjustment also has the advantage of aligning the beam profiler and its translation stage, eliminating the need for calibration.

Secondly, for the calibration of the other elements, no significant improvements are proposed. Automating this step would improve the speed of the assembly process and more accurate stages could improve the calibration's accuracy. However, this calls for more expensive stages and the current sensitivity of the calibration is sufficient.

Thirdly, and most importantly, the sensitivity of the lateral fibre and GRIN lens alignment is already enough to adjust the position with the necessary precision, even with the relatively large GRIN lens that was used in this setup. The experiment uses a GRIN lens with a diameter about two times larger than current research. This lowers the sensitivity of the measurement because a smaller GRIN lens has a greater refractive index, causing a larger change in the lightpath when a similar position change occurs. The angular sensitivity might be sufficient, but the introduced translations nullify this. For the

	Sensitivity		**Repeatability**
	Goal	Result	
Fibre-beam profiler	-	0.4 deg	+
Fibre-GRIN lens			+/-
Lateral (μm)	3	<1	
Angular (deg)	0.23	0.4	
Separation distance (μm)	5	10	

Table 5.1: Comparison between the set goals and reached results of sensitivity and repeatability

separation distance between the fibre and GRIN lens, the sensitivity of the beam profiler with a pixel width of $5.5\mu m$ is the limiting factor. However, it is still sufficient for an indication of the minimum BD.

Finally, an undesirable aspect in this setup exists to create a testing environment that won't be present in a real assembly procedure. In this test setup, the fibre is clamped onto the housing creating a loose fibre tip which can oscillate due to the vibrations of the vacuum pump. This leads to a significant loss in constancy of measurements in the y-direction lowering the sensitivity.

Repeatability

Overall the setup contains several parts with insufficient stiffness. By using stiffer materials, the setup is more stable and repeatability is improved. The first step in the procedure, the alignment of the fibre and beam profiler, has sufficient repeatability as shown in section 4.1. Although the method is not very accurate, the alignment procedure is robust and sufficiently precise. The most significant improvement would be automating the process to fasten it. The same arguments can be considered for the following step, the calibration of the setup.

In the last step, the alignment of the fibre and GRIN lens, multiple factors can improve the repeatability. While the equipment provides sufficient sensitivity and precision, the current methodology in the research relies on manual optimization, compromising the repeatability. The beam profile is primarily assessed manually by visual inspection lacking sufficient accuracy and reliability. Replacing the manual method with a beam optimization algorithm will ensure more precise analysis and optimization of the beam profile increasing the repeatability. This holds for the lateral alignment, angular alignment and the separation distance of the fibre and GRIN lens.

6

Conclusion and recommendations

To conclude this thesis, the most important findings are summarized and conclusions are drawn. This research was an exploratory study with the aim of improving the assembly methods specified for endoscopic research prototype probes. This led to a simplified problem in which only the optical path is researched. The results discussed in chapter 5 show the potential of this method, and future research may advance the method into the field of endoscopic prototypes. This research focuses on the optical path because the rest of the probe is built around it, even among different modalities and recent innovations. After studying the assembly procedure of optical components the following conclusions are presented:

1. A systematic method for selecting the preferred assembly sequence is determined based on the alignment and bonding relations among the optical parts. This also includes an analysis of manufacturing tolerances in relation to the optical path and the resulting errors and loss of image quality
2. In this research we conclude that aligning the fibre and GRIN lens is the most critical precision relation to be defined. Concentricity errors of the optical axes of these components have a major impact on optical performance. Therefore an active alignment method is used to align these two parts.
3. Any repositioning of the fibre led to a new GRIN lens position, even though the fibre was clamped into a V-groove. This confirms the theory that placing the fibre into the assembly has a low repeatability and an active alignment procedure is preferred.
4. The results show that the effect of small position changes of the GRIN lens results in large shifts in the beam profile. A lateral shift of $150\mu m$ causes a clearly visible skewed beam profile.
5. The results show that an error of $40\mu m$ in the separation distance results in a changed beam profile. This adds to the conclusion that the manufacturing tolerances ($200\mu m$ for the GRIN lens length) are too large for accurate passive alignment.
6. The pixel width of the beam profiler limits the sensitivity of the alignment process, and the repeatability necessary to determine the separation distance.
7. The accuracies of the stages are sufficient for a repeatable process.

In addition to the third conclusion, it remains unproven that a rotation of the GRIN lens will only cause a shift of the beam profile because of parasitic translations. Using a calibrated setup could prove this theory. To improve the sensitivity of the proposed setup, a beam profiler with a smaller pixel width needs to be introduced. If the beam profiler is not the limiting factor anymore, it probably is the GRIN lens. In this setup, a larger GRIN lens than normally is used and a smaller GRIN lens should show a better sensitivity. Thus increasing the sensitivity even more. The current setup as a proof-of-concept shows sufficient repeatability but to advance the prototypes into the research field, an optimization algorithm should be used to increase the repeatability. To reach this implementation, three suggestions for further research are provided:

1. This research is focused on the alignment of the GRIN lens and fibre and does not include fixing the optical elements to the housing. For a better comparison, this step should be considered.
2. This research investigates all three optical elements for the assembly method but the final setup for alignment does not include the prism. To create prototypes, the alignment of the prism should be studied.
3. The miniaturization of the probes was not compromised in this research. However, it is proposed to investigate the possibilities further.

A

Assembly Orders

All the 15 unique assembly orders are shown in Figure A.1, Figure A.2, Figure A.3 and Figure A.4, where the corresponding tables show the different parts. In five options the fibre and prism are assembled passively first and the GRIN lens is placed between these two parts. This is very prone to errors because a misalignment of either the fibre or the prism can not be accounted for by the alignment of the GRIN lens. Therefore, these five options are discarded. As a result, there are 15 - 5 = 10 valid unique assembly orders. These are shown in Figure A.5, where the step indicated in red shows the step of active alignment. The reason for this choice of active alignment is explained in chapter 2.

In the ten assembly orders, some very similar options exist now the selection for the active alignment of the fibre and GRIN lens is made. To ease the selection procedure, some assembly orders are treated as one. Firstly, it does not influence the result whether the prism or GRIN lens is firstly placed passively in the housing. Therefore, these two options (nr. 3 and nr. 4) are treated as one. Also, in nr. 5, the prism and GRIN lens are passively aligned outside the housing and then joined with the housing, which results in almost the same assembly steps as nr. 3 and nr. 4. Therefore, this order is not treated separately. However, the difference between aligning inside or outside the housing will be investigated if this order is chosen.

Order number 10 also assembles the GRIN lens and prism outside the housing. However, this sub-assembly is combined with the assembly of the fibre and housing and is therefore different. Orders nr. 6 and 9 are very similar because of the decision of passive alignment of the prism. The fibre and GRIN lens are assembled in both designs, and the sub-assembly is put into the housing. The only difference is whether the prism is placed into the housing before or after the sub-assembly. Consequently, these orders are treated as one. This leaves 7 groups of assembly orders to address. Multiple argumentations can be thought of to select the best order of assembly. As explained in chapter 2, the ease of part handling is essential. The fibre is very small, about 125 micrometres, and is very long. Therefore, it is preferred to move the GRIN lens during the active alignment. This discards the orders nr. 2, nr. 3, 4, and 5, and nr. 8, leaving three assembly orders.

Assembly order number 10 is rejected due to the active alignment step coinciding with the placement of the sub-assembly containing the GRIN lens and prism into the housing with the fibre already in place. This makes it challenging to measure intermediate results, particularly with the presence of the prism. Also, relocating the sub-assembly concerning the housing and fibre becomes more difficult. Moving the GRIN lens and prism together, without placing an extra alignment part into the housing is very challenging. Finally, the decision is between aligning the fibre and GRIN lens inside the housing, or outside the housing and relocating it into the housing. Although the fixing of the elements is not taken into account in this selection process, it is important to realize that the fibre and GRIN lens are not necessarily fixed together after the first step of assembly outside the housing. This creates extra challenges concerning the relocation of this sub-assembly. Concluding, because relocation introduces extra handling steps and may introduce new errors and, because there is no clear advantage, assembly outside the housing is discarded. This leaves the first assembly order as the best one.

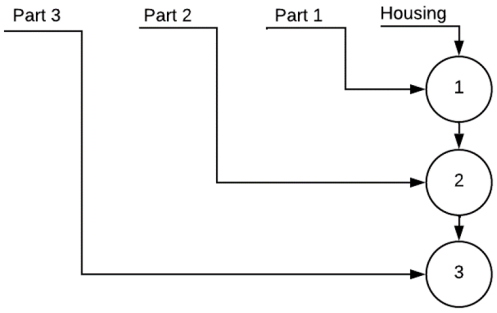

Figure A.1: A figure

	Part 1	Part 2	Part 3
1.	F	P	G
2.	F	G	P
3.	G	P	F
4.	G	F	P
5.	P	F	G
6.	P	G	F

Table A.1: All consecutive assembly orders with the housing as the first part

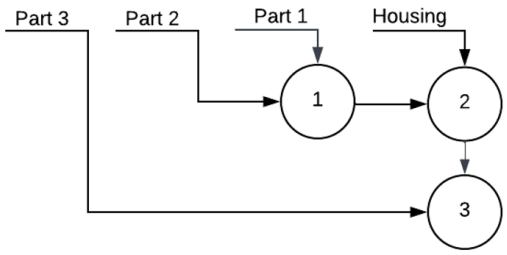

Figure A.2: A figure

	Part 1	Part 2	Part 3
7.	G	F	P
8.	P	F	G
9.	P	G	F

Table A.2: All consecutive assembly orders with the housing as the second part

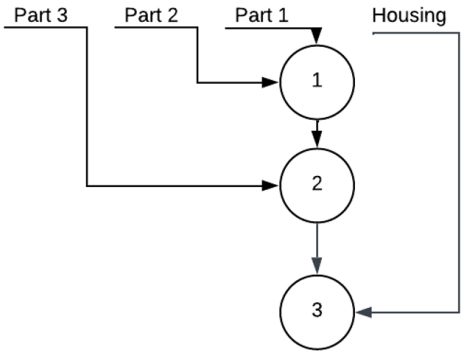

Figure A.3: A figure

	Part 1	Part 2	Part 3
10.	G	F	P
11.	P	F	G
12.	P	G	F

Table A.3: All consecutive assembly orders with the housing as the last part

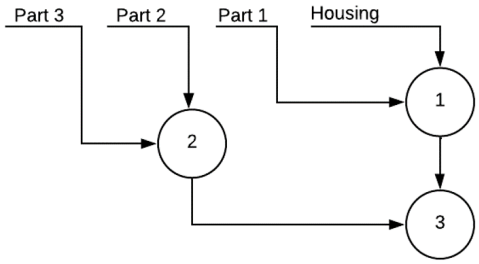

Figure A.4: A figure

	Part 1	Part 2	Part 3
13.	P	G	F
14.	G	P	F
15.	F	P	G

Table A.4: All assembly orders using a subassembly

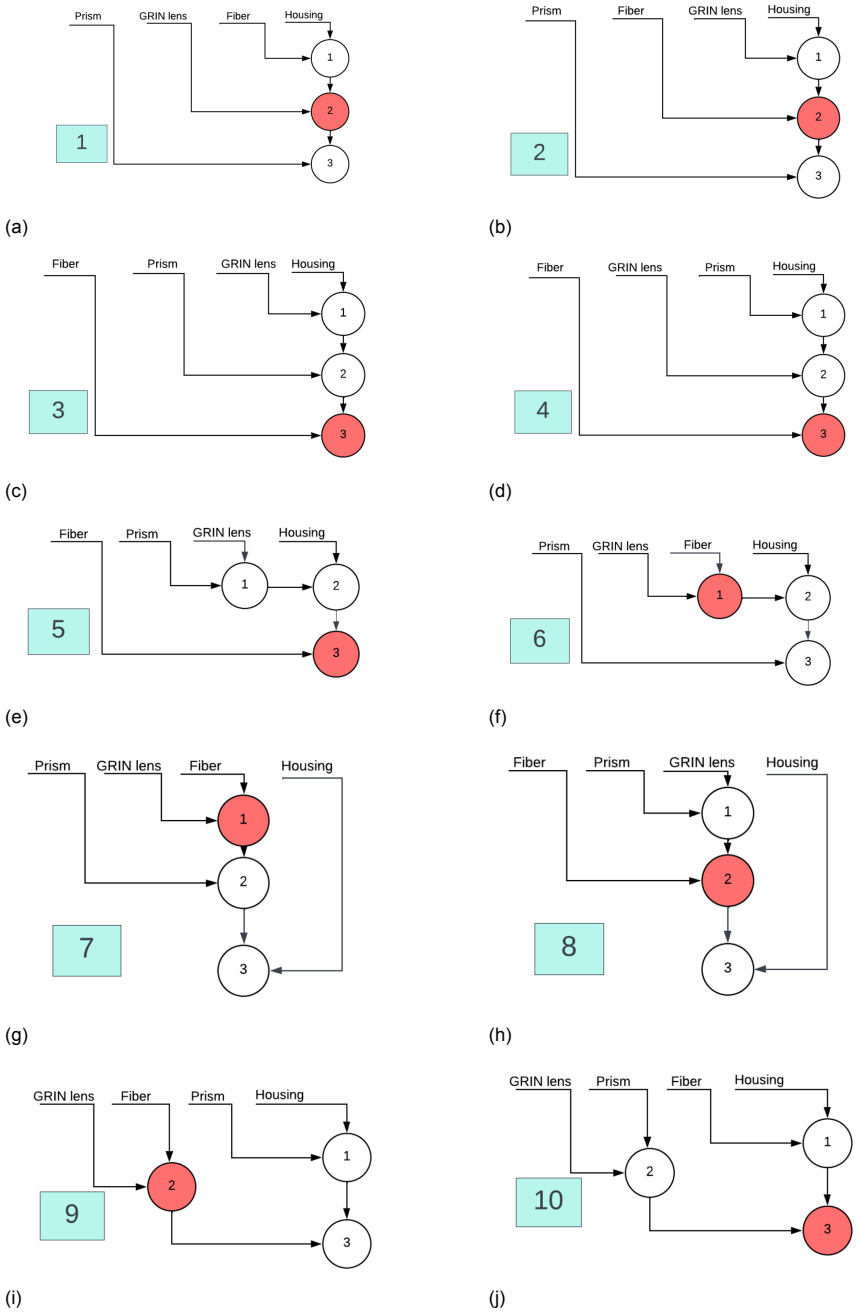

Figure A.5: All viable assembly orders including an active alignment step for the fibre and GRIN lens indicated by the red circle. The numbers in the blue squares are added for clarity of the selection.

B

Orthogonality

Theoretically, there are several ways to determine the alignment of the fibre and beam profiler. These results show why the implementation of additional focusing lenses is necessary. The ways to determine the orthogonality are:

- Beam ellipticity
- Difference between the centre of centroid and peak position
- Change of beam centre when distance changes
- Difference between the Gaussian fit and the real beam profile

Beam ellipticity

The beam ellipticity is not accurate enough to determine the angle. This can be seen in Table B.1, where seven measurements are taken, each after a change of 0.4 degrees, and only at one moment (no averaging). The diameters of the x-axis and y-axis (and thus the effective diameter) are changing, but no clear pattern is visible in this range. For the ellipticity, this is the same. Therefore, if no clear change is visible in a range of 2.8 degrees, this is not a sufficiently good indicator.

Difference between the centre of centroid and peak position

To measure these differences, the average of a 1-minute measurement is taken for four different angles at multiple planes of the beam. This is done because these measurements are necessary for the next method as well, and create more data for this method. To get a clear indication of whether this could be a good indicator, the steps are enlarged, to one degree.

InFigure B.1b it is very clear that the difference between the peak location and the centre location at 262 and 263 degrees is smaller than at 264 degrees. However, the graph for 265 degrees shows excessive deviations. Also, there is no clear difference between the 262 and 263 degrees graphs. However, in Figure B.1a, it is clear that there is less change between the different measured angles. This shows that although there is great variation, the changes are not caused by the different angles.

	Diameter x (μm)	**Diameter y (μm)**	**Effective Diameter(μm)**	**Ellipticity(%)**
1	2233	2101	2167	94,1
2	1919,5	2029,5	1974,5	94,6
3	1969	1925	1947	97,8
4	1908,5	2024	1966,25	94,3
5	1848	1974,5	1911,25	93,6
6	1980	1963,5	1971,75	99,2
7	2194,5	2145	2169,75	97,7

Table B.1: Seven consecutive measurements with a change of 0.4 degrees of the beam profiler

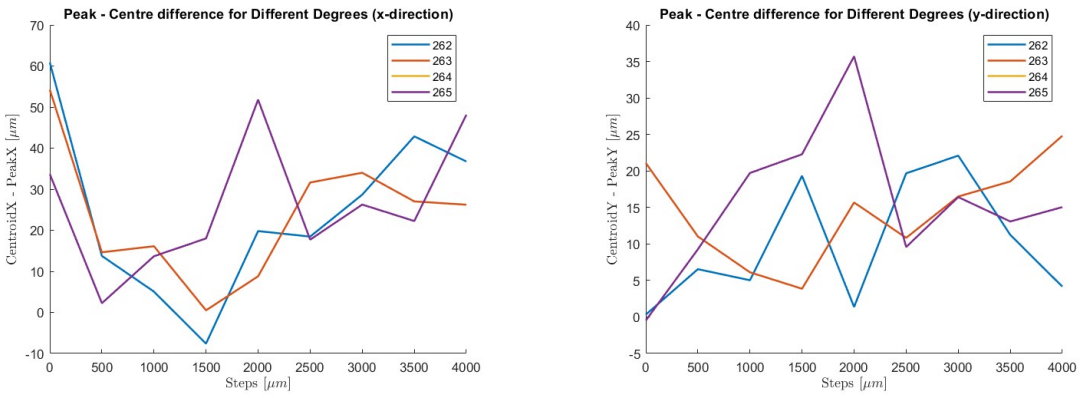

(a) (b)

Figure B.1

When the data is investigated more, the deviations of the peak location change more than the deviations shown, indicating that this parameter is unusable for this goal.

Change of beam centre when distance changes

When the distance between the fibre and the beam profiler is changed, and they are placed under an angle, the centre of the beam will change. Theoretically, for an angle of 1 degree, this change is 8.7 micrometres over a distance of 500 micrometres (tan(1)*500). Although this is less than the range in which the centre is determined in 5 minutes, it is more than the standard deviation. Therefore using a 1 minute average may indicate a better position. This method was proven unusable because there are different coordinate systems and the slope did not change significantly to indicate a misalignment.

Difference between the Gaussian fit and the real beam profile

The final method is to look at the shift in the Gaussian fit. The software of the beam profiler shows a Gaussian fit. After several measurements, we noticed a pattern. Cross-sections at different angles show a shift of the Gaussian fit. Figure B.2 shows an example of various measurements over a rotation of 0.4 degrees. This method might be useful but was not proven more accurate than the method explained in the main text, and it lacks scientific proof. Therefore it was not used in the remainder of this research.

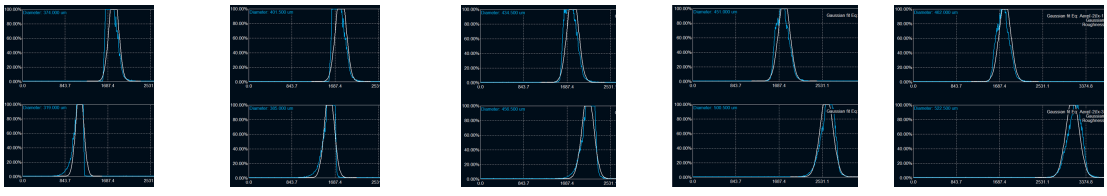

Figure B.2: Gaussian fit over cross-section for 5 different angles, with a change of 0.4 degrees between images. The blue line indicates the cross-section and the white line a Gaussian fit.

C

Additional Results

C.1. Sensitivity of lateral movement of GRIN lens

In Figure C.1 the results of two extra measurements are shown, displaying the influence of the initial setup on the sensitivity and the results of lateral GRIN displacement. The beam profiler is moved to image the beam at a different plane, and the GRIN lens is moved closer to the fibre to create a different working distance and beam diameter. This shows that the change in the beam's centre depends on the location of the imaging plane, which is expected because the angle of the beam causes the change. With a different separation distance between the fibre and GRIN lens, the change is almost the same, which is also expected, as only the beam diameter and working distance change, but the lateral displacement still causes the same angled beam.

C.2. Sensitivity of angular movement of GRIN lens

The relation from the angular movement is challenging to define; therefore, three graphs for each movement are shown. Figure C.2a and Figure C.3a display the relation between the angular movement and the change of the beam's centre in the x-direction, Figure C.2b and Figure C.3b for the y-direction, and Figure C.4 shows the position of the beam's centre for both angular displacements.

C.3. Sensitivity of separation distance fibre-GRIN lens

When the separation distance changes, the centre position changes due to a difference in coordinate systems. The centre's change is visualized in Figure C.5. This image shows the difference in coordinate

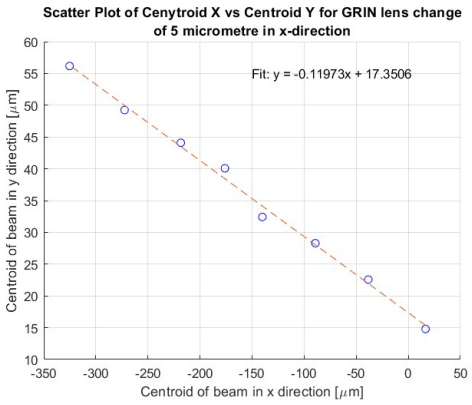

(a) Plot of beam centre after lateral displacement of the GRIN lens in x-direction with steps of $5\mu m$; imaging takes place at a different imaging plane in z-direction

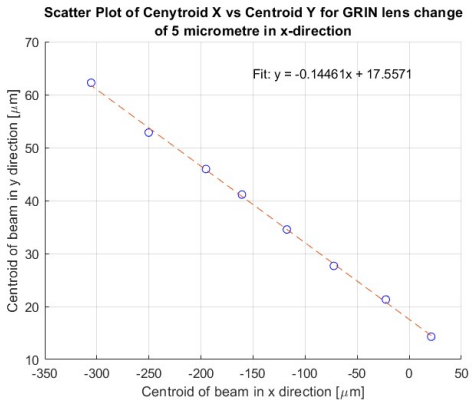

(b) Plot of beam centre after lateral displacement of the GRIN lens in x-direction with steps of $5\mu m$; imaging with a different working distance

Figure C.1: Influence of setup on the results of the lateral displacement of the GRIN lens

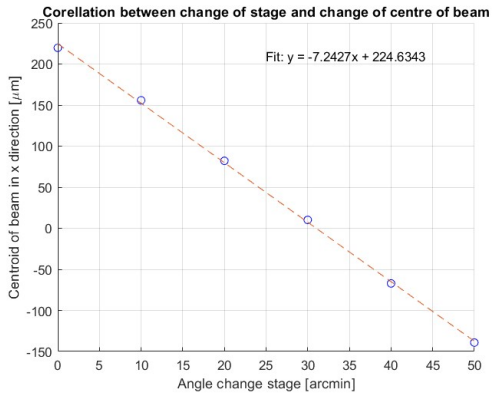

(a)

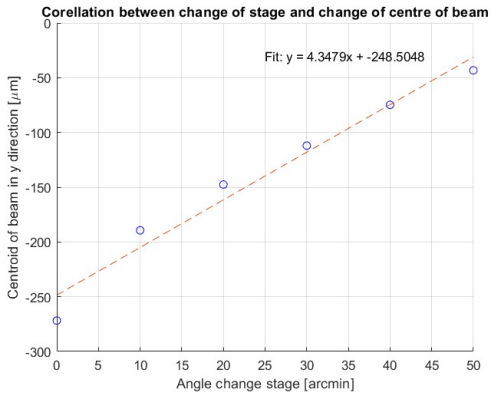

(b)

Figure C.2

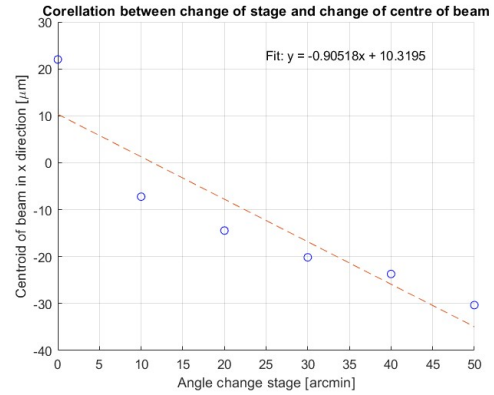

(a)

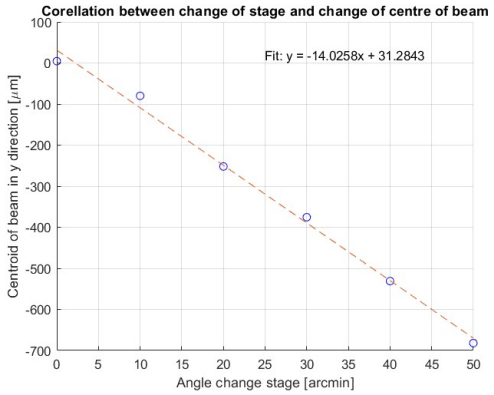

(b)

Figure C.3

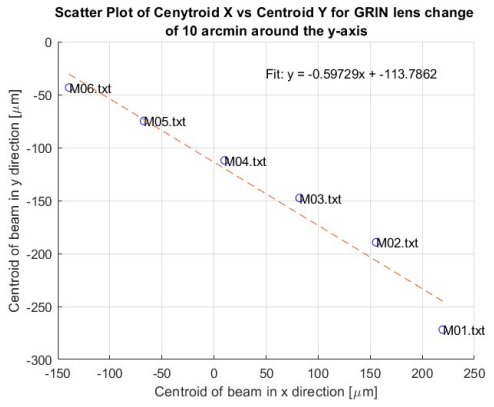

(a)

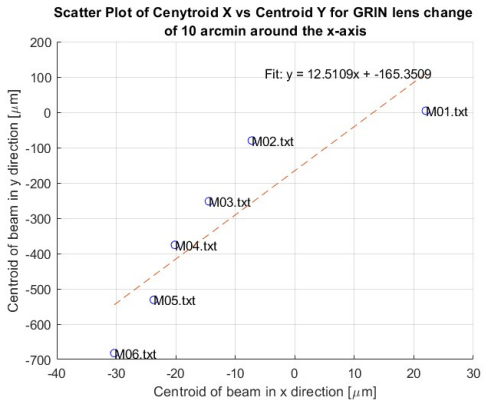

(b)

Figure C.4

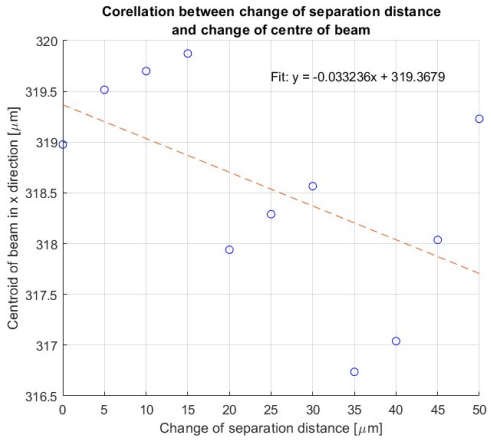

(a) Correlation between separation distance and beam centre in x-direction

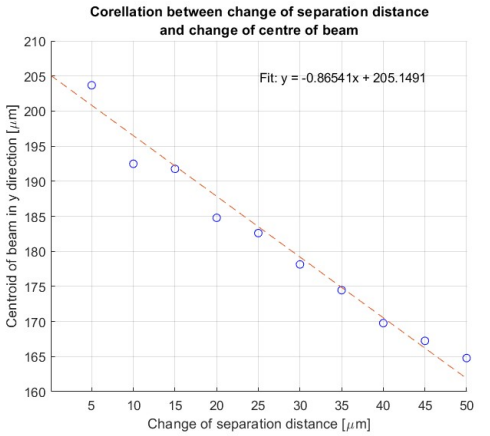

(b) Correlation between separation distance and beam centre in y-direction

Figure C.5: Correlation between separation distance and beam centre

systems is mainly affecting the y-direction.

Bibliography

[1] Axel Boese et al. *Endoscopic Imaging Technology Today*. May 2022. DOI: 10.3390/diagnostics12051262.

[2] Yingchun Cao et al. “High-sensitivity intravascular photoacoustic imaging of lipid-laden plaque with a collinear catheter design”. In: *Scientific Reports* 6 (2016). ISSN: 20452322. DOI: 10.1038/srep25236.

[3] Xianjin Dai et al. “Miniature endoscope for multimodal imaging”. In: *ACS Photonics* 4.1 (Jan. 2017), pp. 174–180. ISSN: 23304022. DOI: 10.1021/acsphotonics.6b00852.

[4] M Daimon, M Shinoda, and T Kubo. “Focusing properties of gradient-index lens for laser-diode beam”. en. In: *Appl. Opt.* 23.11 (June 1984), p. 1790.

[5] Can Duan et al. “Probe alignment and design issues of microelectromechanical system based optical coherence tomography endoscopic imaging”. In: *Applied Optics* 52.26 (2013). ISSN: 15394522. DOI: 10.1364/AO.52.006589.

[6] Adam Filipkowski et al. “Nanostructured gradient index microaxicons made by a modified stack and draw method”. In: *Optics Letters* 40.22 (Nov. 2015), p. 5200. ISSN: 0146-9592. DOI: 10.1364/ol.40.005200.

[7] Adam Filipkowski et al. “World-smallest fiber-GRIN lens system for optofluidic applications”. In: *Photonics Letters of Poland* 8.2 (2016), pp. 36–38. ISSN: 20802242. DOI: 10.4302/plp.2016.2.03.

[8] K H Fuchs. “Minimally invasive surgery”. en. In: *Endoscopy* 34.2 (Feb. 2002), pp. 154–159.

[9] Woonggyu Jung et al. “Numerical analysis of gradient index lens–based optical coherence tomography imaging probes”. In: *Journal of Biomedical Optics* 15.6 (2010), p. 066027. ISSN: 10833668. DOI: 10.1117/1.3523374.

[10] Simon Kretschmer et al. “A bimodal endoscopic imager in a glass package”. In: *Journal of Micromechanics and Microengineering* 28.10 (July 2018). ISSN: 13616439. DOI: 10.1088/1361-6439/aaceb5.

[11] Guangyao Li, Zhendong Guo, and Sung Liang Chen. “Miniature Probe for Forward-View Wide-Field Optical-Resolution Photoacoustic Endoscopy”. In: *IEEE Sensors Journal* 19.3 (Feb. 2019), pp. 909–916. ISSN: 1530437X. DOI: 10.1109/JSEN.2018.2878801.

[12] Teng Ma et al. “A review of intravascular ultrasound-based multimodal intravascular imaging: The synergistic approach to characterizing vulnerable plaques”. In: *Ultrasonic Imaging* 38.5 (Sept. 2016), pp. 314–331. ISSN: 10960910. DOI: 10.1177/0161734615604829.

[13] Youxin Mao. “Analytical method for designing gradient-index fiber probes”. In: *Optical Engineering* 50 (9 Sept. 2011), p. 094202. ISSN: 0091-3286. DOI: 10.1117/1.3626206.

[14] Yanis Taege et al. “Manufacturing and assembly of an all-glass OCT microendoscope”. In: *Journal of Micromechanics and Microengineering* 31.12 (Dec. 2021). ISSN: 13616439. DOI: 10.1088/1361-6439/ac2d9d.

[15] W J Tomlinson. “Aberrations of GRIN-rod lenses in multimode optical fiber devices”. en. In: *Appl. Opt.* 19.7 (Apr. 1980), pp. 1117–1126.

[16] B.E. de Vries. “Possibilities of a generic assembly method for miniaturized endoscopic probes”. Internal TU Delft report: unpublished. (2023).

[17] Chi Wang et al. “Further analysis of focusing performance of an ultra-small gradient-index fiber probe”. In: *Optical Engineering* 53.1 (Jan. 2014), p. 013106. ISSN: 0091-3286. DOI: 10.1117/1.oe.53.1.013106.

[18] Y. Xu et al. “Design and development of a 3D scanning MEMS OCT probe using a novel SiOB package assembly”. In: *Journal of Micromechanics and Microengineering* 18.12 (2008). ISSN: 09601317. DOI: 10.1088/0960-1317/18/12/125005.

[19] Qifa Zhou and Zhongping Chen. *Multimodality imaging: For intravascular application*. Springer Singapore, Jan. 2019, pp. 1–273. ISBN: 9789811063077. DOI: 10.1007/978-981-10-6307-7.